TECHNICAL REPORT RK-73-14

CHEMICAL LASER FLOW SIMULATION AND MIXING STUDIES USING HOLOGRAPHIC FLOW VISUALIZATION TECHNIQUES

C. R. Wimberly
Mechanical Engineering Department
The University of Mississippi
University, Mississippi 38677

L. B. Thorn and G. W. Butler
Chemical Laser Function
Propulsion Directorate
US Army Missile Research, Development and Engineering Laboratory
US Army Missile Command
Redstone Arsenal, Alabama 35809

28 August 1973

Approved for public release; distribution unlimited.

U.S. ARMY MISSILE COMMAND
Redstone Arsenal, Alabama

UNCLASSIFIED

Security Classification

DOCUMENT CONTROL DATA - R & D

(Security classification of title, body of abstract and indexing annotation must be entered when the overall report is classified)

1. ORIGINATING ACTIVITY *(Corporate author)*
US Army Missile Research, Development and Engineering Laboratory
US Army Missile Command
Redstone Arsenal, Alabama 35809

2a. REPORT SECURITY CLASSIFICATION
Unclassified

2b. GROUP
NA

3. REPORT TITLE

CHEMICAL LASER FLOW SIMULATION AND MIXING STUDIES USING HOLOGRAPHIC FLOW VISUALIZATION TECHNIQUES

4. DESCRIPTIVE NOTES *(Type of report and inclusive dates)*
Technical Report

5. AUTHOR(S) *(First name, middle initial, last name)*

C. R. Wimberly, L. B. Thorn, and G. W. Butler

6. REPORT DATE	7a. TOTAL NO. OF PAGES	7b. NO. OF REFS
28 August 1973	52	1

8a. CONTRACT OR GRANT NO.	9a. ORIGINATOR'S REPORT NUMBER(S)
b. PROJECT NO. (DA) 1T662609A308	RK-73-14
c. AMC Management Structure Code No. 662609.11.47300	9b. OTHER REPORT NO(S) *(Any other numbers that may be assigned this report)*
d.	

10. DISTRIBUTION STATEMENT

Approved for public release; distribution unlimited.

11. SUPPLEMENTARY NOTES	12. SPONSORING MILITARY ACTIVITY
None	Same as No. 1

13. ABSTRACT

This report is a summary of work directed toward an understanding of mixing processes in the reaction cavity of a chemical laser device. Holographic optical techniques are used to visualize the flow of gases exiting from an array of supersonic nozzles in a cold flow simulation of the chemical laser. The reconstructed holograms are used to evaluate the mixing process as a function of thermodynamic parameters, flow obstructions, and mass injection mechanisms. Analysis of the mixing is discussed and related to the flow conditions illustrated by shadowgrams, schlieren, and interferograms. Some conclusions are drawn with respect to factors that affect the mixing process.

1 Chemical Lasers -- Flow fields

2. Holography

DD FORM 1 NOV 68 1473 REPLACES DD FORM 1473, 1 JAN 64, WHICH IS OBSOLETE FOR ARMY USE.

UNCLASSIFIED

Security Classification

14. KEY WORDS	LINK A		LINK B		LINK C	
	ROLE	WT	ROLE	WT	ROLE	WT
Chemical laser flow fields						
Double-nozzle cold-flow device						
Photographic impressions						
50-gram device						
Cold-flow device						

CONTENTS

FOREWORD

This report is the final presentation of the efforts and results of the work performed during the summer 1973 under the basic agreement DAHC04-72-A-0001 between the US Army Research Office, Durham, and Battelle Memorial Institute, Columbus Laboratories. The work was performed for the Propulsion Directorate, Chemical Laser Function under the direction of Dr. Walter W. Wharton. The authors wish to recognize the contributions to the test program of J. W. Connaughton, Ben F. Wilson, and others for their part in the conception and design specification of the flow system, for their assistance in feasibility demonstration, and of Mr. Connaughton for his assistance in conducting the testing.

1. Introduction

In accordance with the requirements of the US Army Research Office (ARO/D) with Battelle Memorial Institute, Columbus Laboratories, this report is a summary of the work performed for the US Army Missile Command, Redstone Arsenal, Alabama (MICOM) from 29 May 1973 to 28 August 1973. With the assistance of Mr. L. B. Thorn and others from MICOM the work included:

a) An investigation of the chemical laser flow fields by running a series of tests in a double-nozzle cold-flow device

b) Production of holograms during the tests for the purpose of creating photographic impressions of the flow

c) Utilization of the holograms for construction of shadowgraphs, schlierens, and interferograms

d) Review and oral presentations on the operation and interpretation of shadowgraphs, schlierens, and interferograms

e) Diagnostic interpretation and analyses of the flow fields from cold-flow tests, the relation to flow in the chemical lasers, and recommendations for enhancing supersonic mixing.

2. Experimental Program

The purpose of the test program was to investigate the mixing of supersonic streams exiting from two dimensional nozzles. The nozzles were designed to provide geometric similarity with respect to the nozzles of the "50-gram device" used in chemical laser experiments. As shown in Figure 1 the nozzles used in the "cold-flow device" include a single full nozzle in the center with two half nozzles on each side. The cold-flow nozzle system was designed to be twice the size of the nozzles used in the hot flow 50-gram device, with the exception of depth. The cold-flow double nozzle device was 5 centimeters deep, while the 50-gram device is only 0.5 inch in depth. The reason for this difference was the low density gases expected in the cold flow model and the reasonably high density level requirement for photography.

a. Equipment, Instrumentation, and Facility

The cold-flow device, housing and instrumentation, is shown in Figure 2(a) and (b). The volume into which the gases flow from the nozzles is designated as the cavity. Pressures and temperatures were measured in the cavity as well as in the chamber upstream of the nozzle throat (designated manifold pressures and temperatures).

The pressure transducers used in the tests were from Consolidated Electrodynamics Corporation (CEC), including two with a pressure range of 0 to 25 psia for manifold pressure measurements and one with a range of 0 to 1 psia for cavity pressure measurements. Mass flow rates were obtained from a sonic nozzle fixed area venturi (obtained from the Fox Valve Company) and calibrated by the NASA/MSFC calibration facility using gaseous helium and nitrogen. Upstream pressure versus mass flow rate calibration curves for these gases were provided. The mass flow rates for actual flow conditions as a function of temperature differences were obtained from the equation

$$\dot{m}_a = \dot{m}_c \sqrt{\frac{T_c}{T_a}} \quad . \tag{1}$$

The calibration curve for methane was obtained from the nitrogen curve and the formula

$$\dot{m}_{CH_4} = \dot{m}_{N_2} \sqrt{\frac{T_{N_2}}{T_{CH_4}}} \frac{\left[\bar{M}\gamma \left(\frac{2}{\gamma+1}\right)^{\frac{\gamma+1}{\gamma-1}}\right]^{1/2}_{CH_4}}{\left[\bar{M}\gamma \left(\frac{2}{\gamma+1}\right)^{\frac{\gamma+1}{\gamma-1}}\right]^{1/2}_{N_2}} \quad . \tag{2}$$

The thermocouples used for temperature measurements were of chromel-alumel with a 1/16-inch stainless steel sheath (ISA type K) at a reference junction of 65.59°C (150°F) and a range of -190°C to 1371°C.

The cold flow device (nozzles, supports, and flow control prongs) and the housing were designed by personnel of MICOM and constructed of aluminum alloy 6061-T6 by the Astrospace Corporation in Huntsville, Alabama. High quality optical glass windows (4 5/8 × 6 5/8 × 3/8 inches), BK-7, coated to reduce glare, with rubber O-rings were used to seal off the test section at opposing sides of the cavity. Smaller glass windows of the same quality were used to cover the ends of the nozzles to assure two dimensional flow through the nozzles. Optical glass was required to assure negligible deflections of laser light used in photographing the flow field. Prior to test initiation the lower glass window was broken and replaced by a window of the same optical quality, but was 1/2 inch thick and uncoated.

The test gases were injected into the manifold by lines entering the system from opposing sides as shown in Figure 2(b). One line was used to inject mixtures of nitrogen and helium through the center nozzle while the other line was used to inject either nitrogen or methane through the outside half-nozzles. The cold flow housing was attached to a vacuum system in the chemical laser laboratory building to provide a low pressure condition in the cavity prior to each run. For some runs wires were placed in the flow and on other runs a mass injecting device was installed to investigate the effects on mixing (see the run sequence in Table 1).

b. Test Sequence and Operations

The test sequence, test conditions, and resulting data are shown in Table 1. As shown, 39 runs were made at 27 different run conditions. Gas mixtures of nitrogen and helium were selected for flow through the center nozzle to provide variations in molecular weight and to simulate the secondary nozzle flow conditions of the 50-gram device. Methane and nitrogen gases were used separately in the outside nozzles to provide variations there. Methane gas was selected because of its agreement in molecular weight and specific heat of the primary nozzle flow conditions of the 50-gram device. The conditions tested included: matched flow rates of the 50-gram device, matched exit pressures, over-expanded flow, conditions causing separated flow in the nozzles, single nozzle flow, matched flow rate per nozzle, and the effects of mass injections and wire obstructions on mixing.

The method of operation for each run began by pumping the cavity and reservoir down to a low pressure condition (2 to 3 torr prior to each run). A countdown was required to allow the optimum charge voltage for the laser (normally 10 seconds to charge). A photographic plate was placed in position just prior to the run. At time zero the valves were opened to provide the desired flow rates and conditions at the nozzle exit. Because transient flow conditions lasted 1 to 2 seconds, the laser was fired 7 to 8 seconds after flow initiation. The normal run time was about 10 seconds.

c. Holographic System

The complete holographic flow visualization system entails three basic subsystems consisting of (1) the hologram forming optics, (2) the pulsed ruby laser, and (3) the reconstruction system. Figures 3 and 4 show the functional relationships between the components. A ruby laser pulse generates the coherent information beam necessary for making the holograms. As shown, the beam passes through a beam-splitter and separates into an object beam and a reference beam. The object beam makes a double pass through the cavity via a spherical mirror and is recombined with the reference beam at the photographic plate. The recorded fringe pattern or transmission hologram contains

the desired information about the flow structure in the cavity and this information is reconstructed upon illumination by a similarly coherent beam. The hologram may be reconstructed as either a shadowgram, a schlieren, or an interferogram (a double exposure is required for making an interferogram).

The hologram forming optics were designed and provided by Sci-Metrics Inc. of Tullahoma, Tennessee. It is a double-pass, off axis, spherical mirror system designed to have better than 1/4 wavelength overall distortion at 6943 Å. The cavity windows were of high quality optical glass whose surfaces were parallel and flat to within $\lambda/6$. The photographic plate (Agfa-Gevaert 10E75) was illuminated through a relay operated shutter that opens for 1/30 second and simultaneously closes a microswitch to initiate the laser 30-nanosecond burst. The pulsed ruby laser system was a Korad K-1 series used in the Q-switched mode. Referring to Figure 3 it is seen that the cavity rear element consists of a pockel cell, Brewster stack, and a 99-percent rear reflector. The front reflection and laser cavity output element is a temperature variable Fabry-Perot etalon. The etalon acts as a longitudinal mode selector to give greater temporal coherence. Beam spatial coherence is achieved by the use of an intracavity transverse mode selector approximately 3 millimeters in diameter. This aperture was placed at the initial lasing position when the laser was operated at its threshold input voltage. The beam spatial coherence was further improved by a spatial filter utilizing a 5X microscope objective lens that focuses the beam through a 50-micron pinhole. The combination of these optical elements and the quality of the ruby rod give sufficient coherence for good hologram quality.

Figure 4 shows the basic optical arrangement for reconstruction of the developed hologram. A Spectra-Physics Model 124A He-Ne gas laser with 15 milliwatt output and TEM_{∞} operation provides the coherence needed for faithful reconstruction.[1] The beam is expanded using a spatial filter and illuminates the hologram through a collimating lens. The reconstructed image may then be photographed as a shadowgram or a schlieren, depending of course upon the insertion of a knife edge at the focus. Schlieren views, both parallel and perpendicular to the flow, were reconstructed by cutting the beam from the vertical or the horizontal directions, respectively.

The television camera (with objective lens removed) as shown in Figure 5 was found useful for preliminary optical adjustments in the reconstruction process. The reconstructed image was later diverted by a second mirror to a camera (not shown) for permanent photographic recording.

---

[1] Collier, Burkhardt, and Lin, Optical Holography, Academic Press, New York, 1971, pp. 170-174.

3. Flow Field Analysis

In the effort to understand the characteristics of the flow and the mixing phenomena, the analytic portion of this study involved (1) a theoretical evaluation of the flow using the physical characteristics of the nozzles, known flow points and test data obtained during the runs and (2) diagnostic evaluation of the photographs reconstructed from holograms. From an assumption of inviscid nozzle flow some theoretical values of the flow conditions at the nozzle exits were obtained. For example, by knowing the exit to throat area ratio (from Figure 1) for the cold flow nozzles, the exit Mach numbers were calculated (for one dimensional isentropic flow) from the following equation, assuming sonic velocity at the throat

$$\left(\frac{A_e}{A_t^*}\right)^2 = \frac{1}{M_e^2}\left[\frac{2}{\gamma+1}\left(1+\frac{\gamma-1}{2}M_e^2\right)\right]^{\frac{\gamma+1}{\gamma-1}} \quad . \tag{3}$$

For many of the runs with $A_e/A_t^* = 5.872$ and $\gamma = 1.38$ to 1.67 (ranges for methane to helium) respective exit Mach numbers were from $M_e = 3.3$ to 4.1. For other runs, where the cavity pressures were high, lower Mach numbers occurred at the exit.

From the measured pressures in the manifold (assumed to be near the stagnation conditions) the exit pressures were also estimated (again from one dimensional isentropic flow) from the equation,

$$\left(\frac{A_t^*}{A_e}\right) = \frac{\left[1-\left(\frac{P_e}{P_o}\right)^{\frac{\gamma-1}{\gamma}}\right]\left(\frac{P_e}{P_o}\right)^{1/\gamma}}{\left(\frac{\gamma-1}{2}\right)^{1/2}\left(\frac{2}{\gamma+1}\right)^{\frac{\gamma+1}{2(\gamma-1)}}} \quad . \tag{4}$$

For the same area ratio and range of γ, the exit to stagnation pressure ratio range was (for many runs) from $P_e/P_o = 0.00065$ to 0.00125 (for helium and methane, respectively). Some exit pressures, based on run conditions, photographs, and Equation (4), are listed in the test data.

The temperatures at the exit were approximated from the energy equation with the assumption that the manifold conditions are near

stagnation and that the gases were ideal which results in the standard temperature equation

$$T_e = T_o \left(1 + \frac{\gamma - 1}{2} M_e^2\right)^{-1} \quad . \qquad (5)$$

T_o is the measured manifold temperature and M_e is the exit Mach number calculated from Equation (3). Exit temperature of the gases from this equation for the nozzles ranged from 83° to 91°K.

Maximum values of the velocity at the nozzle exit plane was obtained from the definition of the Mach number

$$V_e = \sqrt{\gamma R T_e}\, M_e \quad . \qquad (6)$$

The exit velocities ran from about 2100 feet per second for nitrogen and methane to about 6200 feet per second for pure helium. Approximations of the density at the exit were obtained from the ideal gas equation of state

$$\rho_e = \frac{P_e}{R T_e} \quad . \qquad (7)$$

These state property conditions at the exit were determined as only approximations and for idealized conditions, but provided a basis for qualitative evaluation. For many of the runs the relatively high cavity pressure levels reduced the exit Mach number and in some cases moved the shock inside the nozzle (particularly for runs involving wire obstructions and the mass injection tests). The photographs of the tests were useful in this respect and also provided a comparison of predicted and actual effects.

Single nozzle effects were run to establish the maximum dimensions of the mixing zones. Because of the relatively low cavity pressures for most runs the free plume intersection regions were considered to provide approximate zones where mixing would most likely occur. This provided a reasonable approximation, although the actual mixing zones would be a function of turbulence levels and transverse momentum of the gases there.

It was learned from the tests that mixing can be retarded by shocks in the flow; while we know that, in parallel streams, mixing can be increased through turbulence and diffusion of particles in the mixing zone. Turbulence levels, however, will vary according to the relative velocities and Reynolds numbers of the parallel streams. Gases of low molecular weights, such as helium used in the test, have higher velocities (other conditions remaining the same) at the exit and in the plume than gases with high molecular weights. High velocity differences of the mixing streams will increase vorticity at the interface, induce turbulence, and thus enhance mixing. The level of turbulence created will also influence the width of the mixing zone; however, probably the greatest influence on the extent of turbulent mixing would be the amount of transverse momentum the gases have in the regions where mixing is occurring. Turbulent mixing is also considered to provide a greater effect (in mass units) than mixing by molecular diffusion. From these considerations the photographs were viewed to locate and isolate turbulent zones and thus to depict areas of greatest mixing.

Figures 6, 7, and 8 (run number 6 at condition 1 from Table 1) are a shadowgraph, and two schlieren, respectively, for cold flow conditions that closely match the hot flow from the 50-gram device. Figures 7 and 8 are schlieren, respectively, made with the knife edge sitting in a vertical position parallel to the flow, traversing horizontally, and in the horizontal position, perpendicular to the flow and traversing vertically. Figure 9 (run 4, condition 4) is an interferogram of the same flow conditions. In these views, the exit and cavity pressures are nearly the same providing a near isentropic flow condition. The molecular weight of the center nozzle and flow rates for both nozzles are also matched with the 50-gram device. Calculated exit conditions for this run show some velocity differences between the flow conditions at the exit of the respective nozzles, but are not considered to be sufficient for good mixing. Figures 10 and 11 (run 13, condition 5), which are a shadowgraph and a schlieren, respectively, are also near the flow conditions of the 50-gram device. For this run the outside nozzle flow conditions match the flow rate, molecular weight specific heat and velocity of the primary nozzle (molecular weight was a little lower and the exit velocity was a little higher than that produced by the secondary nozzle of the 50-gram device). As shown however, from the basis for determining mixing in the plumes, a similar conclusion can be drawn, as was from the previous figure that only partial mixing is occurring for these run conditions.

Deviations from the flow conditions of the 50-gram device were also performed as indicated in the run sequence. For example, Figures 12 and 13 (run 7, condition 2) and Figures 14, 15, and 16 (run 21, condition 12) are shadowgraphs and schlieren depicting matched flow rates and matched velocity levels at the exit planes of the nozzles. As shown, little mixing occurred for these run conditions initially with some mixing occurring downstream.

The effect of high velocity and Reynolds number differences in nozzle exit conditions is shown in Figures 17, 18, and 19 (run 18, condition 3). Here the mixing zone is much larger than for the other run conditions, the maximum occurring about 2-nozzle diameters downstream. In this run the flow rates in both nozzles match the flow rate conditions in the 50-gram device. The molecular weights, however, were considerably different to provide the differences in exit velocity.

Flow field investigations were also done with wire obstructions in the flow. The purpose of the wires was to enhance mixing. Several wire sizes were investigated, as shown in Figure 20, including sizes 0.02, 0.049, and 0.094 inch in diameter. A 0.03-inch wire was not used. The wires were installed into the cavity at a distance of 0.1- to 0.2-inch downstream of the nozzle exits and symmetrically set across the center nozzle (which was used to represent the secondary nozzle of the 50-gram device). Figure 13 (run 32, condition 21) is a typical example of the effects of the wires in the flow. In this run high velocity differences existed between the nozzles, although the mass flow rates were matched with the 50-gram device. The wires in this run and others considerably altered the flow, increased the cavity pressure, caused separated flow in the nozzles, and significantly reduced the exit Mach numbers and velocities.

A few runs were done with nitrogen mass injection normal to the exhaust flow. The mechanism used in this effort is shown in Figure 22. Four orifices on each side of the device were symmetrically placed to inject the nitrogen slightly downstream (0.1 to 0.2 inch) of the nozzle exit and into the stream of each nozzle. A pressure of three times the freestream stagnation pressure (manifold pressure) was selected to provide the proper penetration of the jet. An example of the effects of the mass injection tests is shown in Figure 23 (run 24, condition 15).

In this run the mass flow rates matched that of the 50-gram device. As shown, the mass injection completely disrupted the flow, pushing the shock far into the nozzle, and reducing the cavity to highly turbulent subsonic flow.

4. Conclusions

With reference to the agreement with the Battelle Memorial Institute, all tasks outlined in the scope of work were completed. With regard to the experimental program several conclusions can be drawn:

a) The cold-flow device can be used to qualitatively investigate hot flow nonreacting gases in a chemical laser with the following reservations.

1) The half nozzles on each side of the device provide two possible distortions in reviewing the data and photographs. The boundary layer along the wall and shock reflections from the wall will affect the flow conditions not present in the hot-flow device.

2) The 5-centimeter depth of the cold-flow device caused blending of the effects viewed in a photograph. For perfectly designed nozzles and zero misalignment, this would not be a problem and from the photographs taken, it did not appear that this caused any major distortion.

3) The small glass windows covering the nozzles assured two dimensional flow through the nozzles; however, there were no flow control devices in the cavity. Aft of the nozzle exit, the flow (for many runs) expanded in three dimensions, causing difficulties in analyzing the flow there.

b) Flow field matching of the 50-gram device in the cold-flow device indicated only partial mixing of the supersonic stream.

c) Deviations in run conditions significantly affected the mixing phenomena, with maximum mixing occurring when velocity and Reynolds number differences (between adjacent nozzles) were the greatest.

d) Wire in the flow and mass injection into the stream were very effective in causing mass disruption of the flow in the cavity; however, detailed effects on mixing using these devices are inconclusive.

5. Recommendations

Recommendations are as follows:

a) In an unobstructed flow, high Reynolds numbers and their differences in mixing streams cause the greatest potential for mixing. This can be accomplished by combination of molecular weights, mass flow rates, and/or differences in the exit to throat area ratio. For example, decreasing molecular weights can increase the velocity, but will also decrease the density. Mass flow rates may have to be increased or alternating nozzles could be designed for varying exit to throat area ratios to provide the desired flow differences for optimum mixing.

b) As suggested from a), an optimization study should be performed (based on a range of probable molecular weights in the primary and secondary nozzles, ranges of probable flow rate and nozzle design) to provide the greatest potential conditions for mixing.

c) For small nozzles as are currently being used in lasing experiments, viscous effects in the nozzle can be a potential problem area. With the low density exit conditions the boundary layer at the exit can be quite thick and could extend completely across the nozzle exit, causing difficulties in the mixing in the cavity. Such problems can be helped some by proper nozzle contour design and should be considered in future design.

d) Because the wire obstructions were somewhat effective in the flow field disturbance, further studies may provide means for mixing the flow using obstructions in the flow. Because of the few runs, using mass injection, little can be said, except that this may also provide a means for mixing; however, further studies would have to be run before any recommendations could be made. A potential problem area using obstructions in the flow and mass injection is the effects on the chemical kinetics in the cavity. The relaxation time and the nonequilibrium conditions of the flow should be investigated if obstructions are inserted into the flow.

TABLE 1. TEST DATA (MEASURED)

Run	No.	Condition	$\dot{m}$ Center (grams/sec)		$\dot{m}$ Outside (grams/sec)		Center (psia)	Center (°C)	Outside (psia)	Outside (°C)	Cavity (torr)	Cavity (°C)	Remarks	
			N_2	He	N_2	CH_4	P_{m_c}	T_{m_c}	P_{m_o}	T_{m_o}	P_c	T_c	P_j (psia)	Wires (in.)
1	397	1	0	0	0	-	-	-	-	-	-	-	-	-
2	398	1	30.6	2.10	20.85	-	-	7.5	10.5	21.5	11.25	9.0	-	-
3	399	2	22.4	0.35	22.75	-	-	7.5	11.4	21.5	9.4	9.0	-	-
4	400	4	30.5	2.03	22.75	-	-	7.5	11.44	21.5	11.85	9.0	-	-
5	401	3	17.8	5.15	23.40	-	23.5	10.0	11.88	22.0	29.5	12.5	-	-
6	402	1	30.6	1.83	21.75	-	2.25	10.1	10.80	22.0	11.5	12.7	-	-
7	403	2	24.6	0.55	22.75	-	7.125	10.1	11.38	21.9	14.0	12.7	-	-
8	404	5	28.1	5.35	-	21.2	6.63	10.0	14.0	21.2	19.0	11.5	-	-
9	405	6	28.1	5.26	-	0	6.50	10.0	-	21.5	6.25	12.0	-	-
10	406	7	0	0	-	21.2	-	10.0	13.88	21.2	12.75	12.0	-	-
11	407	8	22.8	0	-	21.2	-	10.0	13.75	21.2	12.75	12.0	-	-
12	408	8	22.8	0	-	21.2	-	10.5	14.0	21.5	12.75	12.0	-	-
13	409	5	28.0	5.30	-	21.5	21.13	7.0	14.55	17.8	28.5	8.8	-	-
14	410	8	22.7	0.80	-	21.5	10.50	7.0	14.75	19.0	20.0	8.8	-	-
15	411	8	22.8	0	-	21.5	10.50	7.0	14.90	18.2	20.01	8.8	-	-
16	412	11	9.8	0	-	21.5	4.50	7.8	13.63	17.8	15.0	8.8	-	-
17	413	X	31.4	6.7	23.0	-	21.13	10.2	11.10	21.5	26.0	11.5	-	-
18	414	3	18.2	15.1	23.0	-	25.0	10.2	11.10	21.5	35.0	11.5	-	-
19	415	9	19.5	15.0	23.0	-	17.0	10.2	11.05	21.5	29.75	11.5	-	-
20	416	10	19.5	15.5	0	-	17.63	10.2	0	21.5	17.0	11.5	-	-
21	417	12	10.0	0	9.88	-	4.50	10.8	4.75	22.0	10.0	11.5	-	-
22	420	13	10.0	0	9.88	-	4.50	10.8	4.75	22.0	29-50	12.0	-	-
23*	421	14	0	14.9	22.7	-	16.0	9.5	10.8	20.8	38.75	11.5	31.0	-
24*	422	15	18.8	13.1	23.1	-	24.25	9.5	11.0	20.0	45.0	11.5	33.0	-
25*	423	16	32.0	0	23.3	-	15.13	9.5	11.0	20.0	33.5	11.5	33.0	-
26*	424	17	0	15.0	0	-	17.0	9.5	1.6	19.8	28.5	11.5	32.2	-
27*	425	17	0	15.5	0	-	17.5	9.5	1.6	20.8	27.75	11.5	32.6	-
28*	426	18	17.6	15.9	0	-	25.0	10.2	1.5	20.2	34.0	11.5	33.0	-
29*	427	19	24.0	0	23.4	-	11.0	10.2	11.0	21.0	26.0	12.0	32.8	-
30*	428	16	32.0	0	23.4	-	15.2	10.2	11.1	20.8	29.2	12.2	33.0	-
31	429	20	0	15.4	22.7	-	16.75	9.0	10.8	21.5	29.8	11.0	-	0.090
32	430	21	18.2	17.6	22.75	-	25.00	9.0	11.0	22.8	33.5	11.0	-	0.090
33	431	22	20.2	14.8	20.8	-	16.13	9.0	9.9	20.8	27.7	11.0	-	0.050
34	432	23	18.3	14.8	20.8	-	25.0	9.0	10.6	19.8	36.0	11.0	-	0.050
35	433	24	0	7.3	10.6	-	7.95	9.5	5.05	19.5	14.2	11.0	-	0.050
36	434	25	0	7.4	0	-	7.95	9.5	0	19.8	9.6	11.0	-	0.050
37	435	26	0	15.5	22.3	-	17.85	9.0	10.7	20.8	29.5	11.0	-	0.020
38	436	27	0	7.5	10.9	-	8.0	9.0	5.25	20.8	14.1	11.0	-	0.020
39	437	26	0	15.6	22.7	-	18.13	9.0	10.75	19.8	30.0	11.0	-	0.020

*Mass injections of N_2.

TABLE 2. DATA CALCULATED FROM TESTS

Run	No.	Condition	Center Nozzle					Outside Nozzles				
			(psia) P_e	C_p/C_v	$\bar{M}$	(ft/sec) V_e	P_e/P_c	(psia) P_e	C_p/C_v	$\bar{M}$	(ft/sec) V_e	P_e/P_c
1	397	1	-	-	-	-	-	-	-	-	-	-
2	398	1	-	-	-	-	-	0.1733	-	-	-	0.7965
3	399	2	-	-	-	-	-	-	-	-	-	-
4	400	4	-	1.45	20.1	2702	-	-	1.40	28	2125	-
5	401	3	0.388	-	-	-	0.680	0.196	1.40	28	2125	0.344
6	402	1	-	-	-	2457	-	-	1.40	28	2125	-
7	403	2	-	-	-	2261	-	-	1.40	28	2125	-
8	404	5	0.109	-	-	-	0.298	-	1.38	16	-	-
9	405	6	-	-	-	-	-	-	-	-	-	-
10	406	7	-	-	-	-	-	-	1.38	16	2811	-
11	407	8	-	1.40	28	2125	-	-	1.38	16	2811	-
12	408	8	-	1.40	28	2125	-	-	1.38	16	2811	-
13	409	5	0.349	1.48	13.31	3320	-	0.2401	1.38	16	2811	-
14	410	8	0.173	1.41	23.25	2332	-	-	1.38	16	2811	-
15	411	8	-	1.40	28	2125	-	-	1.38	16	2811	-
16	412	11	0.074	1.40	28.0	2125	-	0.2249	1.38	16	2811	-
17	413	X	-	-	-	-	-	-	-	-	-	-
18	414	3	-	1.58	8.23	4737	-	-	1.40	28	2125	-
19	415	9	-	-	-	-	-	-	1.40	28	-	-
20	416	10	-	-	-	-	-	-	-	-	-	-
21	417	12	-	1.40	28	2125	-	-	1.40	28	2125	-
22	420	13	-	1.40	28	2125	-	-	1.40	28	2125	-
23	421	14	-	-	-	-	-	-	1.40	28	2125	-
24	422	15	0.400	-	-	-	0.460	0.182	1.40	28	-	0.209
25	423	16	0.250	1.40	28	2125	0.385	0.182	1.40	28	-	0.280
26	424	17	0.280	1.67	4.0	-	0.509	0.026	-	-	-	0.048
27	425	17	0.289	1.67	4.0	-	0.538	0.026	-	-	-	0.049
28	426	18	0.413	-	-	-	0.627	0.025	-	-	-	0.038
29	427	19	-	1.40	28	-	-	-	1.40	28	-	-
30	428	16	-	1.40	28	-	-	-	1.40	28	-	-
31	429	20	-	1.67	4.0	-	-	-	1.40	28	-	-
32	430	21	-	-	-	-	-	-	1.40	28	-	-
33	431	22	-	-	-	-	-	-	1.40	28	-	-
34	432	23	-	1.67	4.0	-	-	-	1.40	28	-	-
35	433	24	-	1.67	4.0	-	-	-	1.40	28	-	-
36	434	25	-	1.67	4.0	-	-	-	-	-	-	-
37	435	26	-	1.67	4.0	-	-	-	1.40	28	-	-
38	436	27	-	1.67	4.0	-	-	-	1.40	28	-	-
39	437	26	-	1.67	4.0	-	-	-	1.40	28	-	-

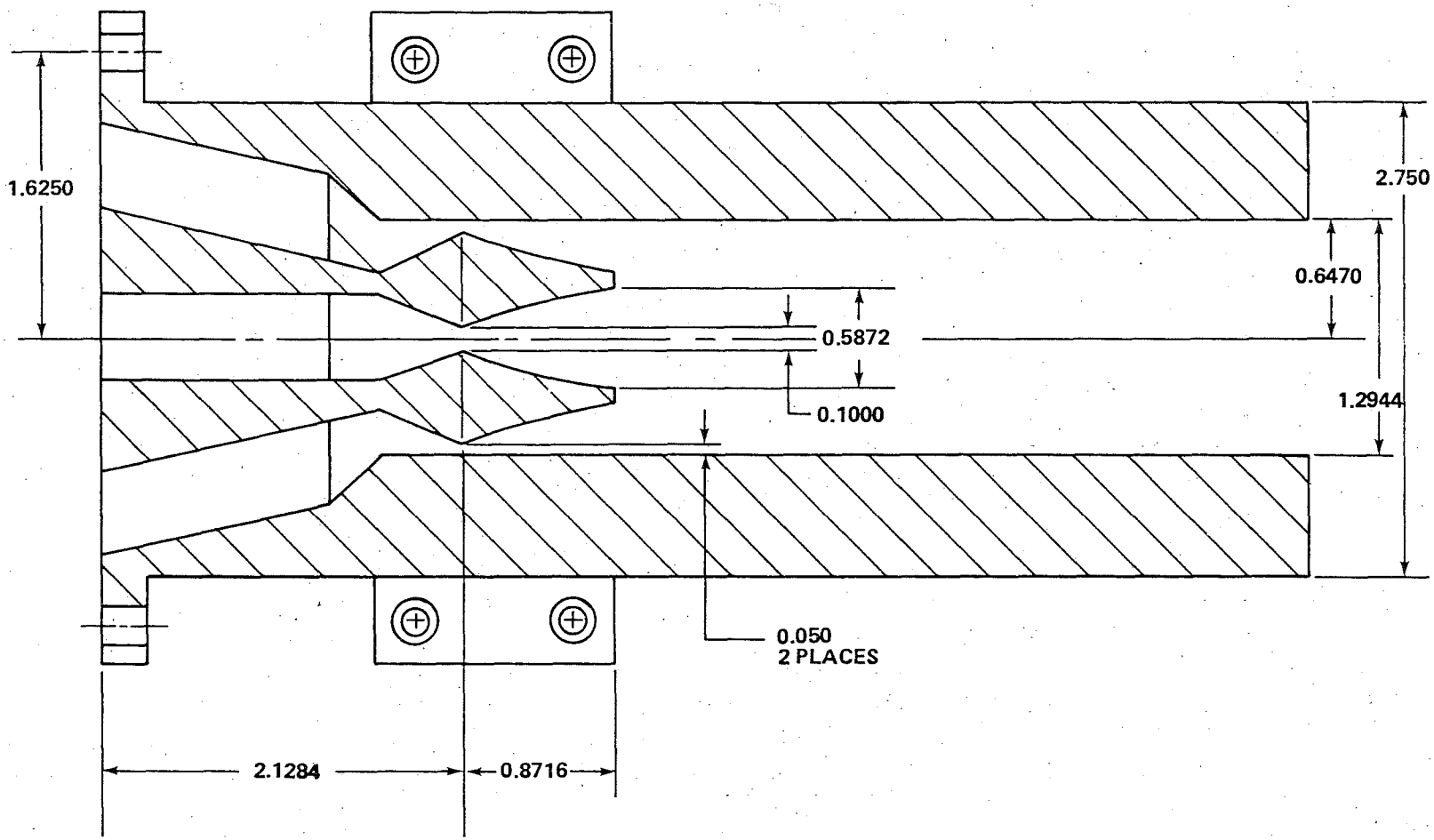

Figure 1. Sketch of the double-nozzle cold-flow device.

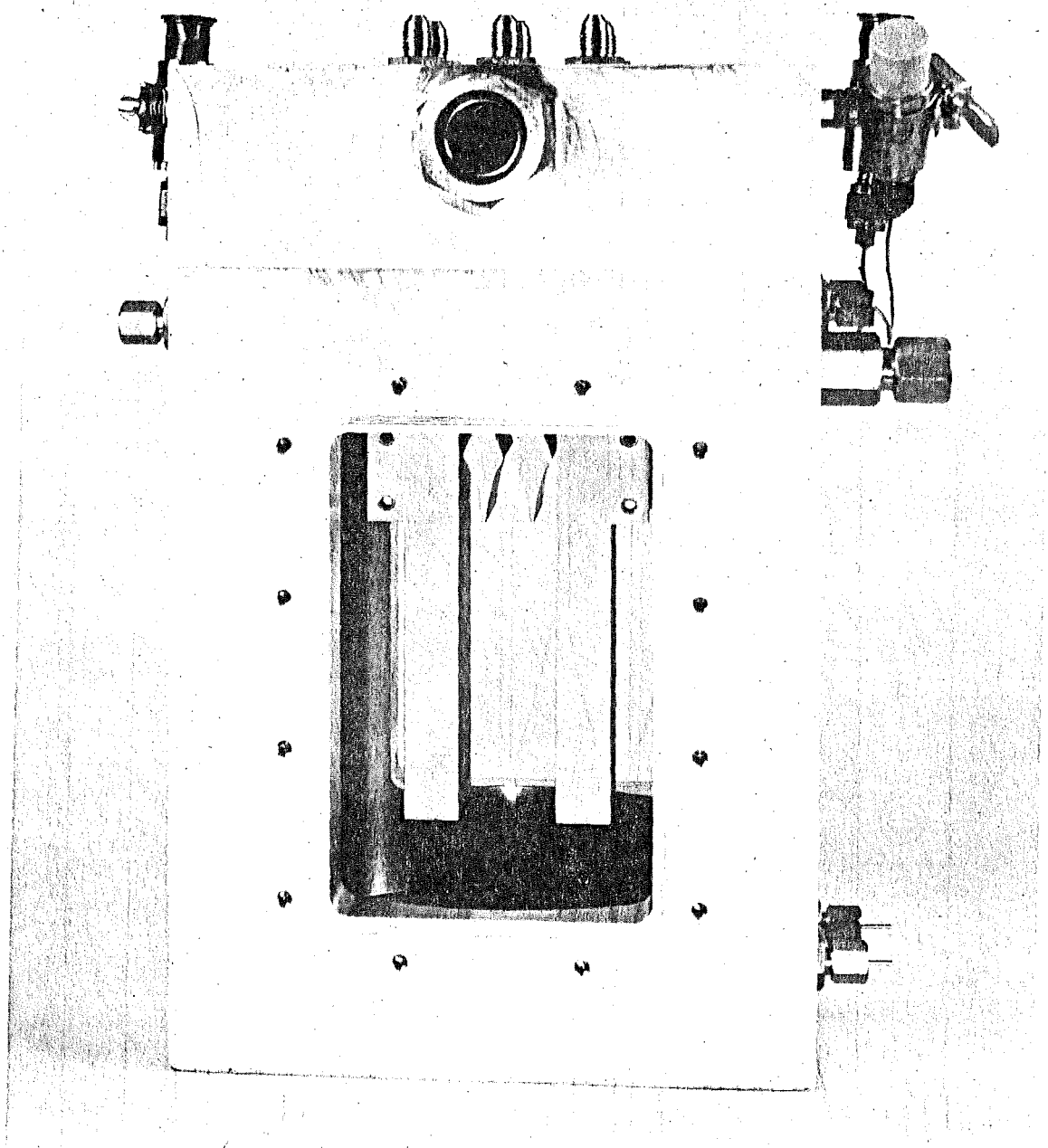

Figure 2. Housing and instrumentation of the cold-flow device.

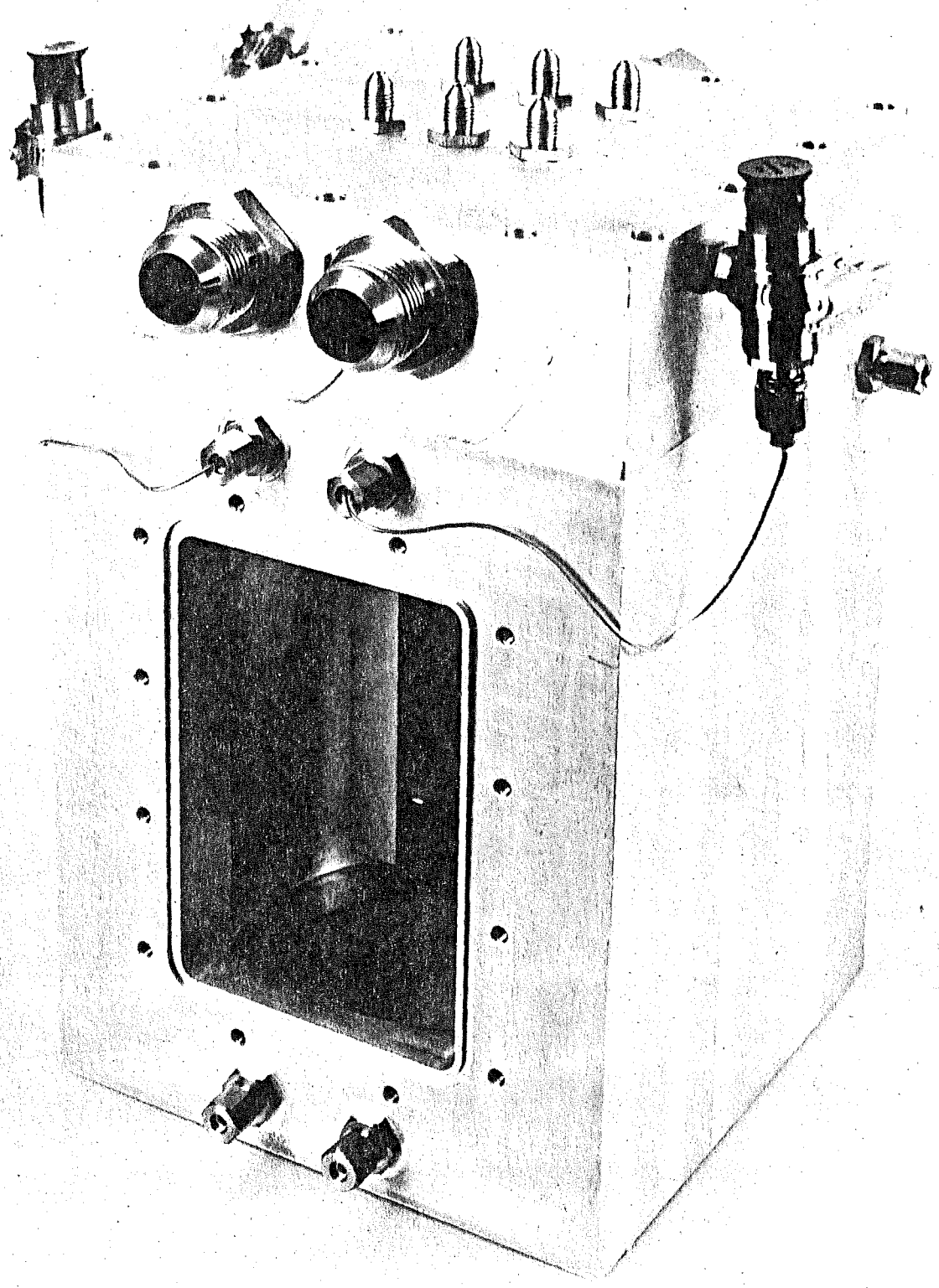

Figure 2. Concluded.

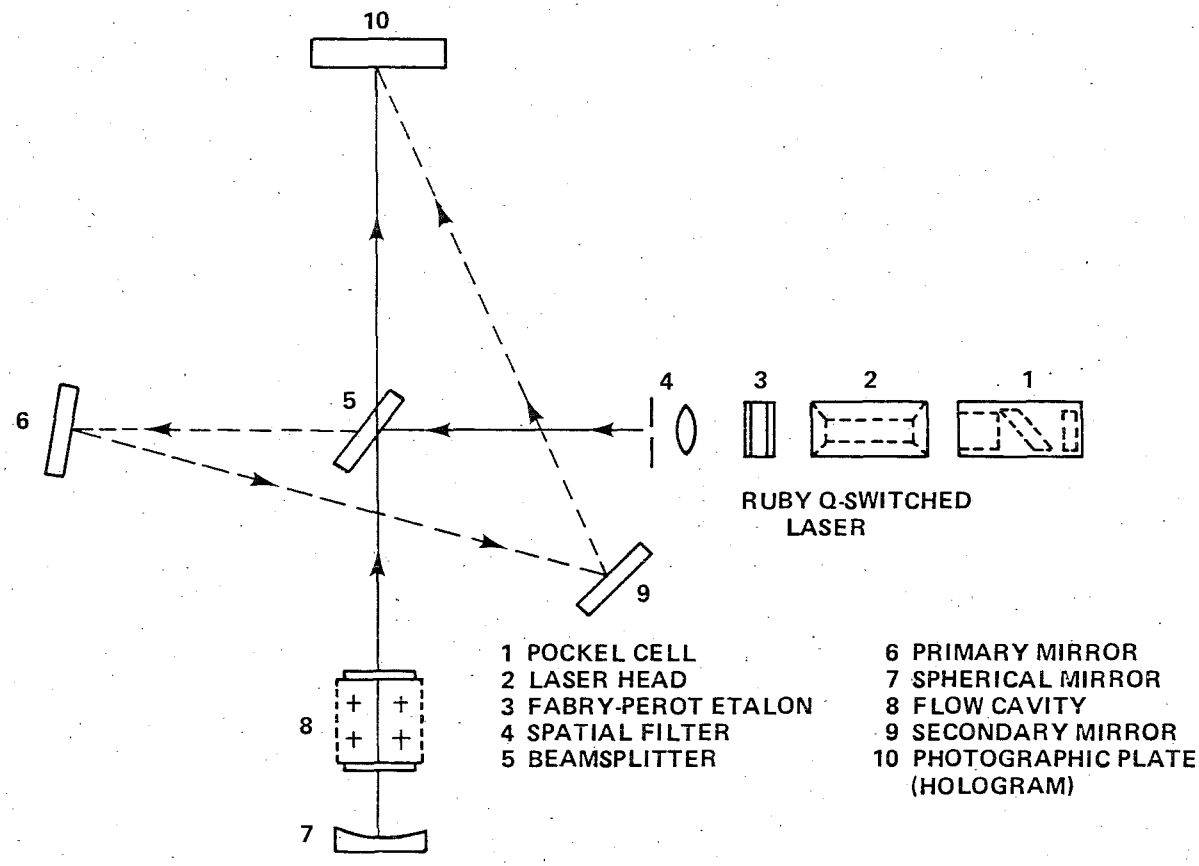

Figure 3. Sketch of the hologram forming optics system.

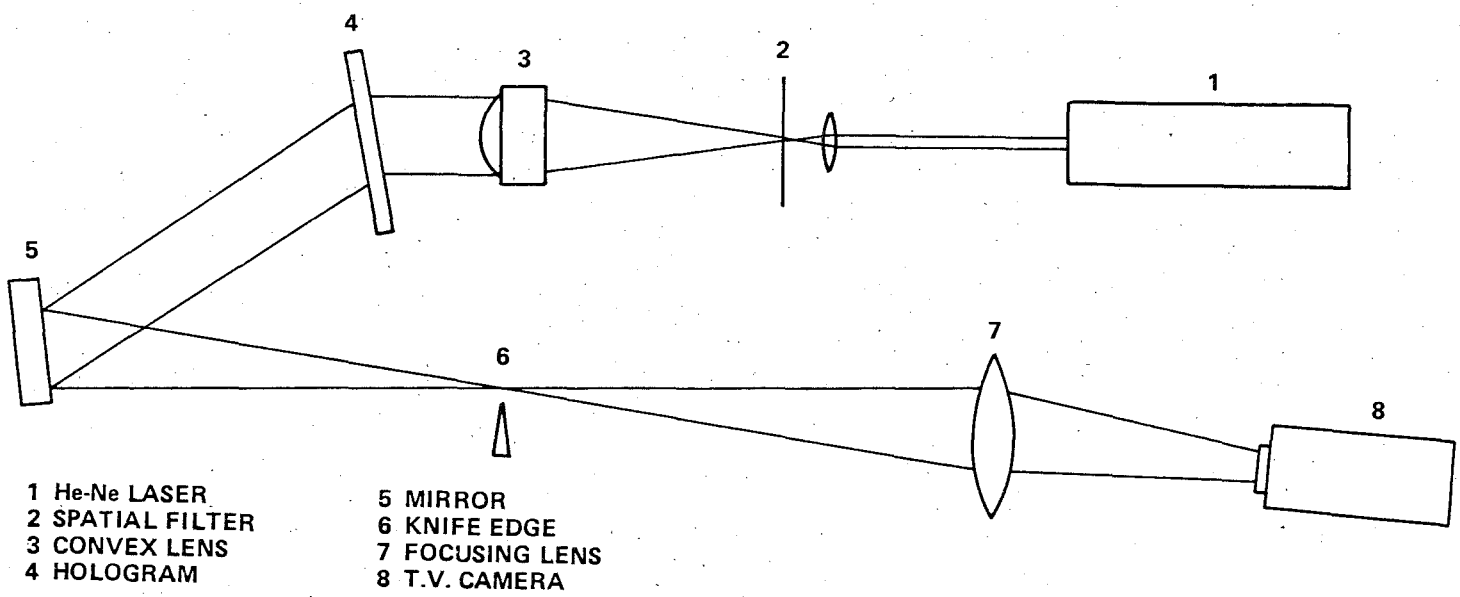

Figure 4. Sketch of the reconstruction optics system.

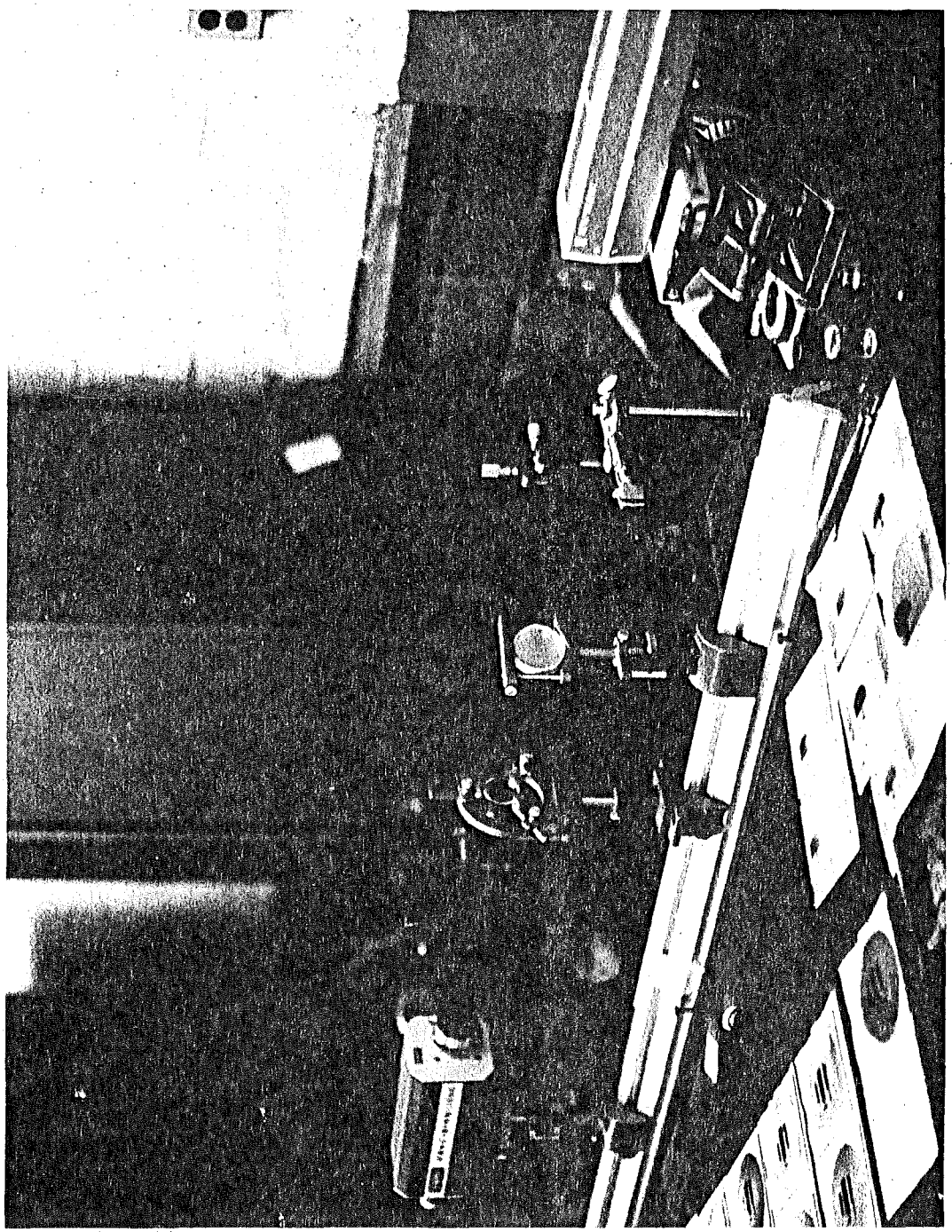

Figure 5. Picture of the reconstruction optics system.

Figure 6. Shadowgraph of run 6, condition 1.

Figure 7. Schlieren of run 6, condition 1 with knife edge set vertically.

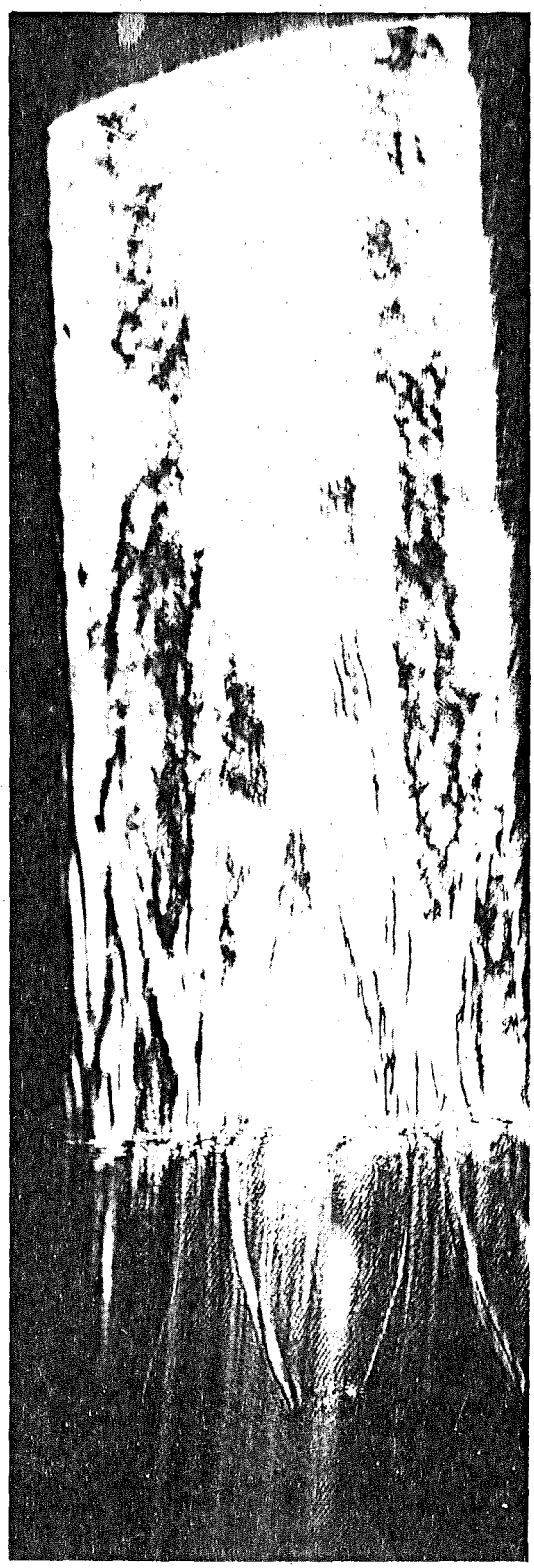

Figure 8. Schlieren of run 6, condition 1 with knife edge set horizontally.

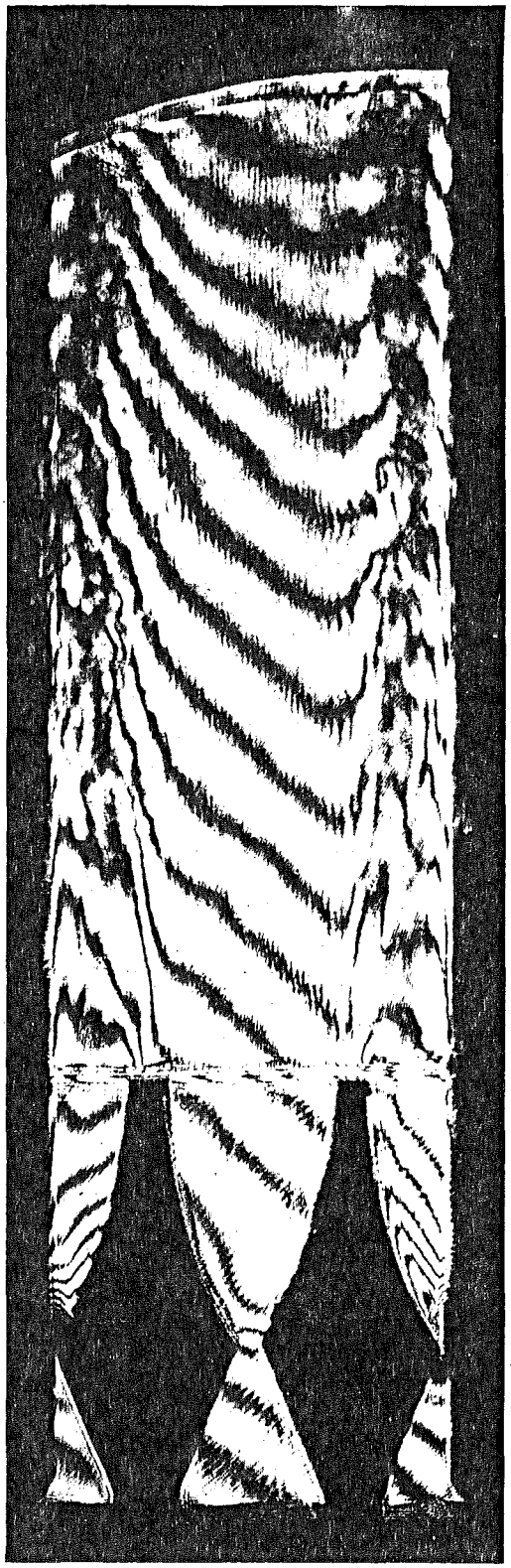

Figure 9. Interferogram of run 4, condition 4.

Figure 10. Shadowgraph of run 13, condition 5.

Figure 11. Schlieren of run 13, condition 5 with the knife set vertically.

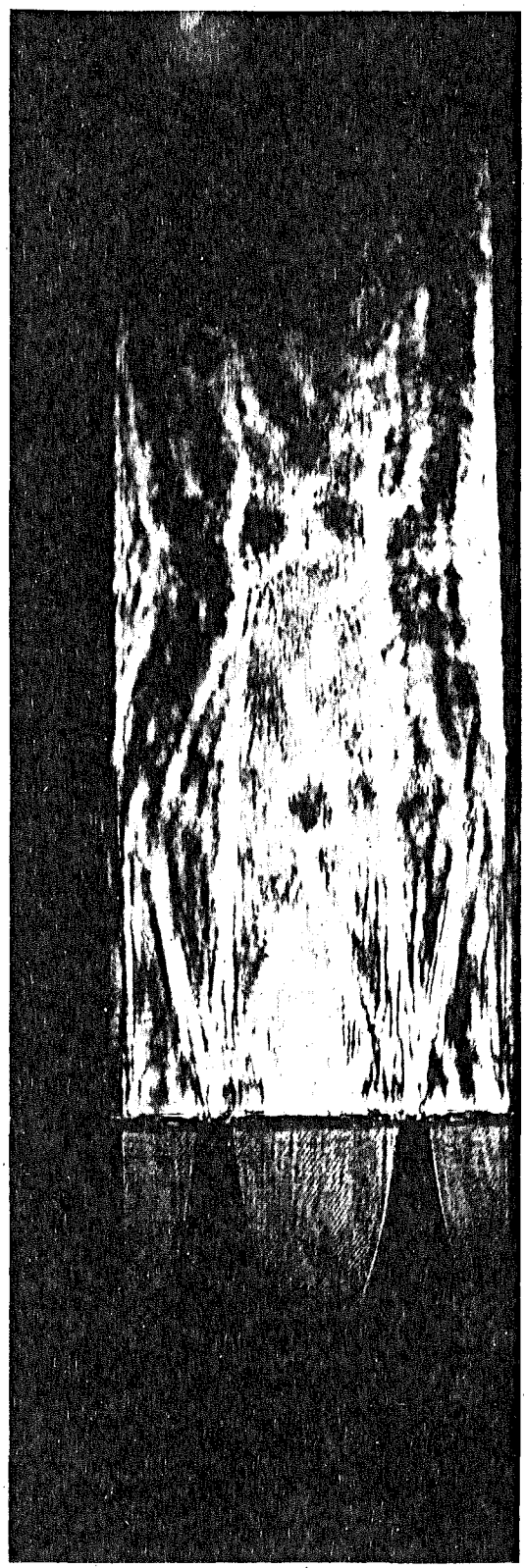

Figure 12. Shadowgraph of run 7, condition 2.

Figure 13. Schlieren of run 7, condition 2 with knife edge set horizontally.

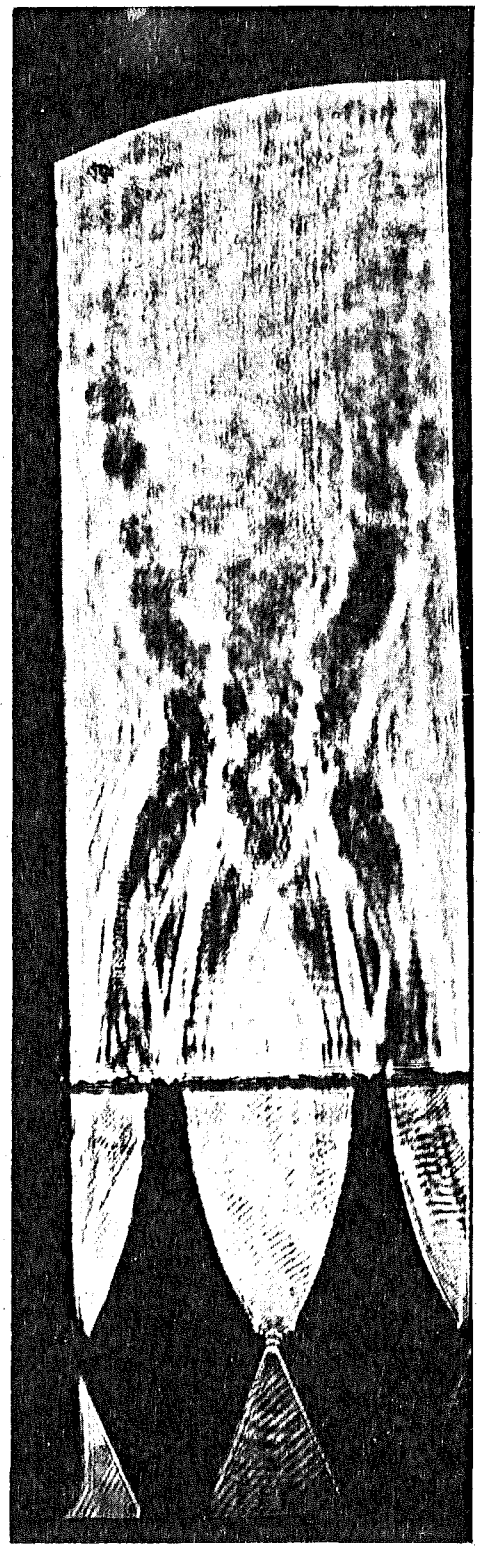

Figure 14. Shadowgraph of run 21, condition 12.

Figure 15. Schlieren of run 21, condition 12 with knife edge set vertically.

Figure 16. Schlieren of run 21, condition 12 with knife edge set horizontally.

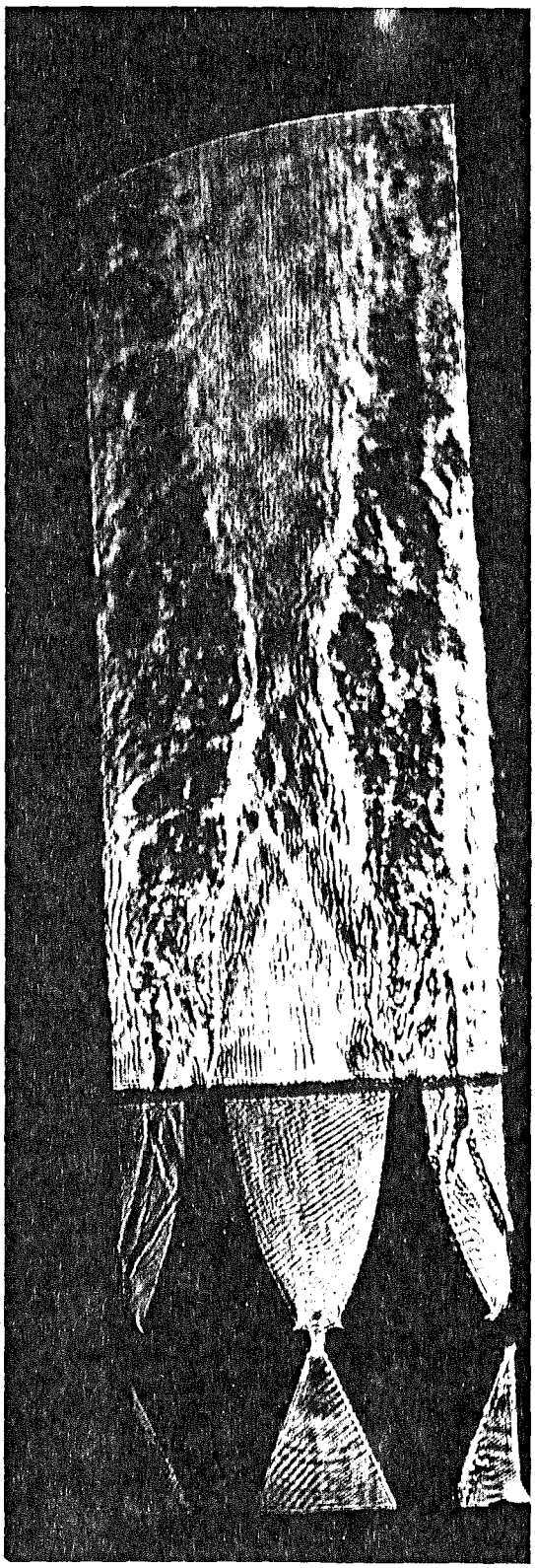

Figure 17. Shadowgraph of run 18, condition 3.

Figure 18. Schlieren of run 18, condition 3 with knife edge set vertically.

Figure 19. Schlieren of run 18, condition 3 with knife edge set horizontally.

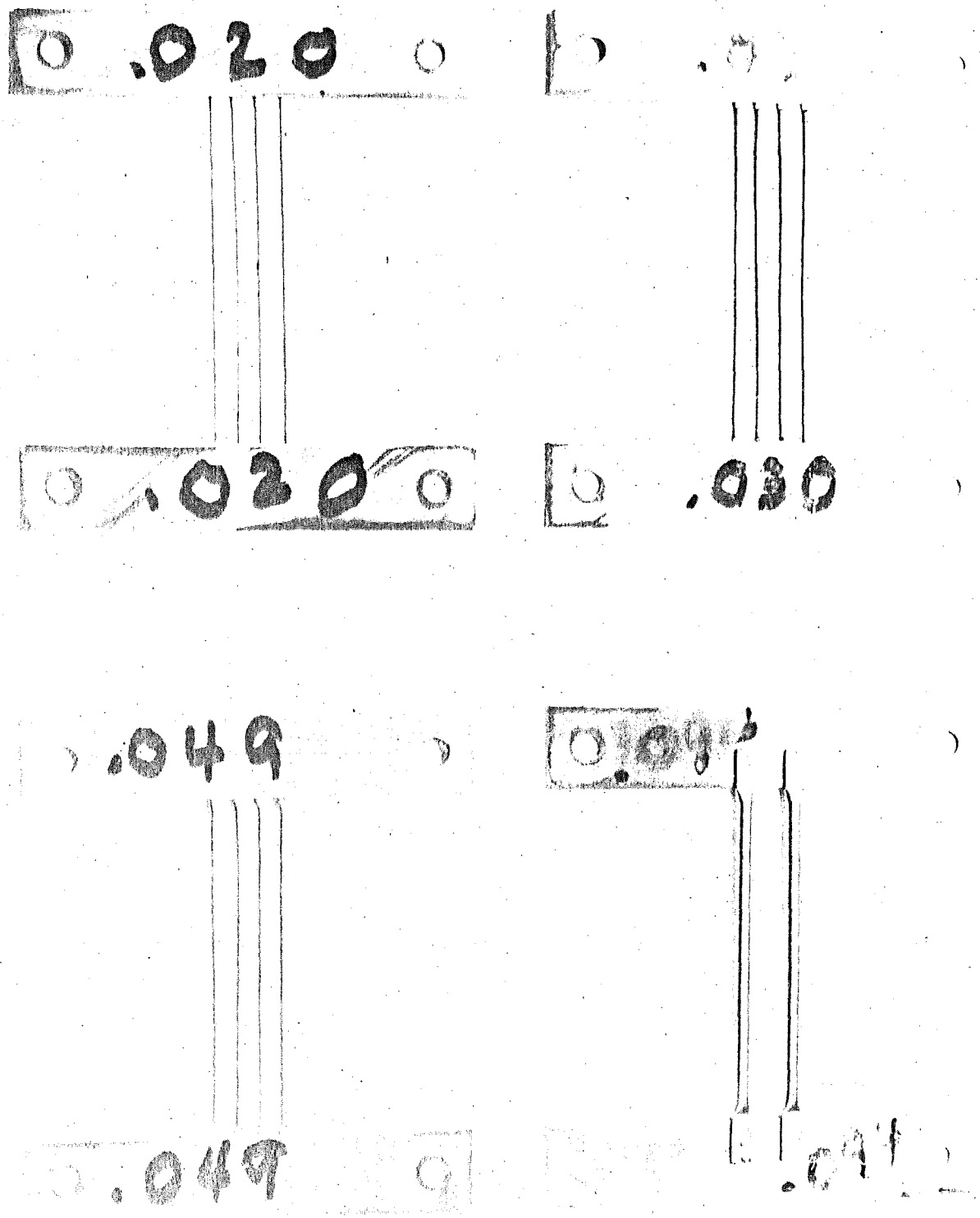

Figure 20. Wire obstruction used in the tests.

Figure 21. Shadowgraph of run 32, condition 21.

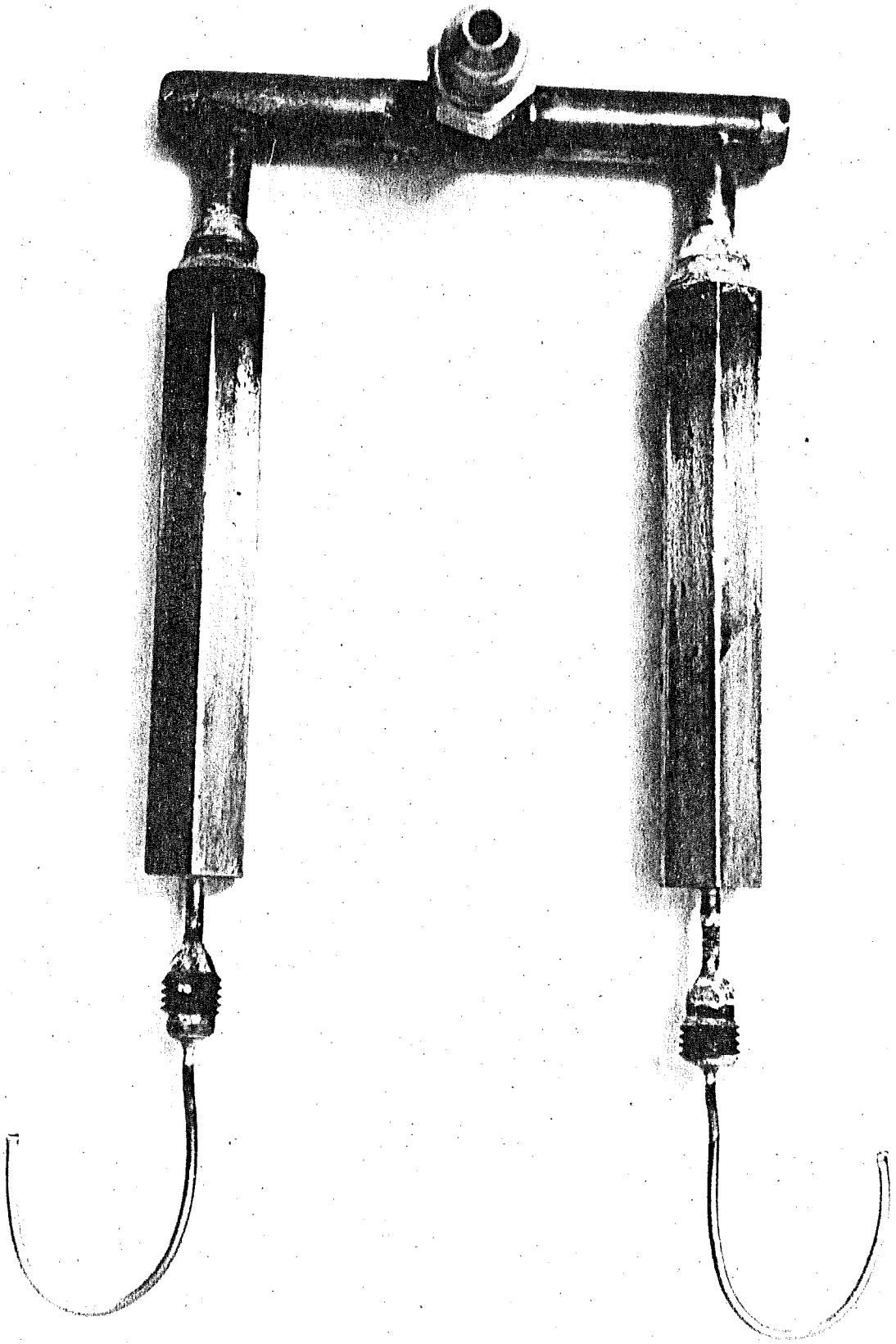

Figure 22. Mass injection device.

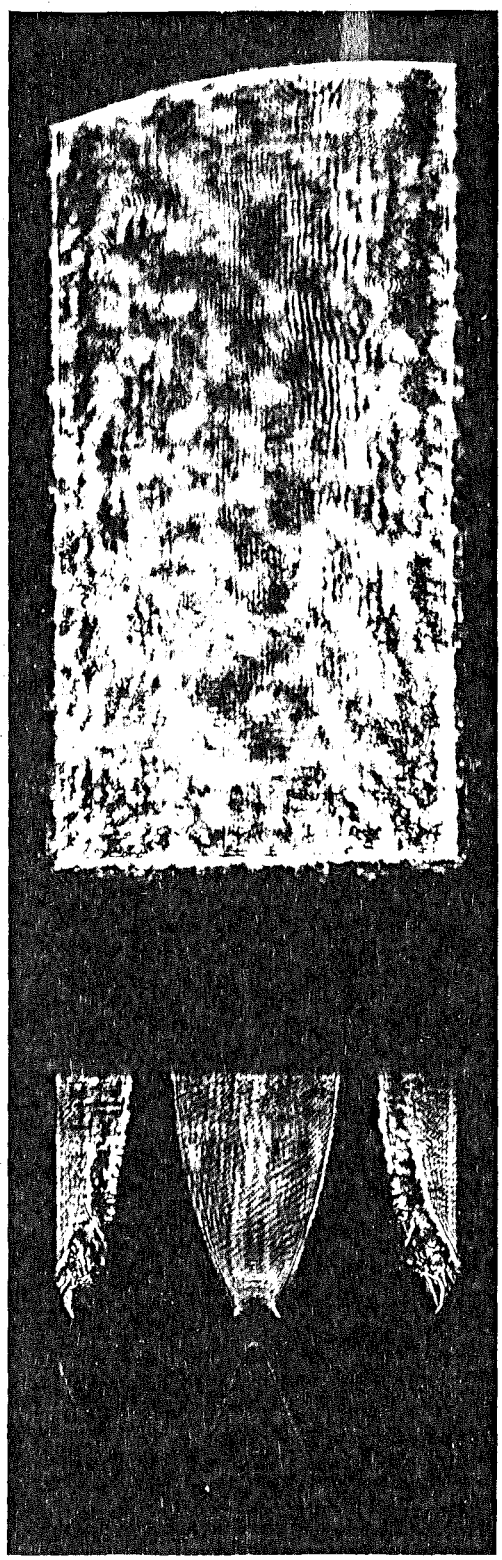

Figure 23. Shadowgraph of run 24, condition 15.

Appendix A.

SHADOWGRAPHS AND SCHLIERENS FUNDAMENTALS

Light Refraction Through a Gaseous Medium

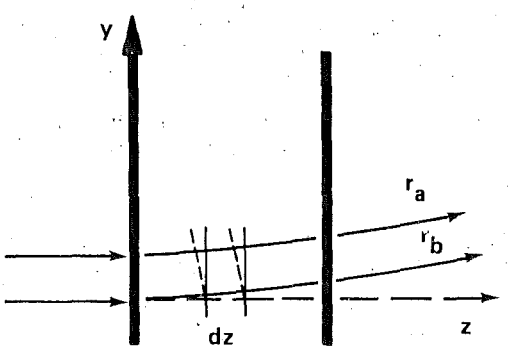

TEST SECTION

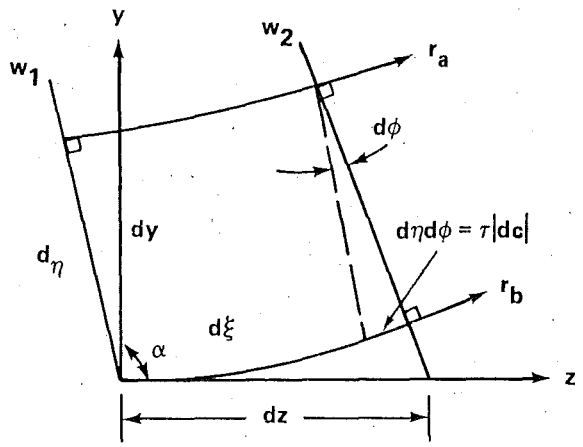

ELEMENT

Definitions:

Density ρ increasing in the positive direction y

n is the index of refraction,

$$n = \frac{C_o}{C}$$

$$= 1 + \frac{\rho\beta}{\rho_s} \quad .$$

Angle of refraction $\epsilon = \int_0^L d\phi$.

From Geometry:

$d\eta = dy \sin\alpha$ $\qquad C = \frac{C_o}{n}$

$d\xi = dz \sin\alpha$ $\qquad \frac{dc}{dy} = -\frac{C}{n}\frac{dn}{dy}$ or $\frac{|dc|}{dy} = \frac{C}{n}\frac{dn}{dy}$

$d\xi$ is distance traveled along r_b. Therefore, $d\xi = \tau C$.

Angle of refraction

$$\epsilon = \int d\phi = \int \frac{\tau |dc|}{d\eta} = \int \frac{\tau |dc|}{dy \sin \alpha}$$

$$\epsilon = \int \frac{\tau}{\sin \alpha} \left(\frac{C}{n} \frac{dn}{dy} \right) = \int \frac{d\xi}{\sin \alpha} \frac{1}{n} \frac{dn}{dy}$$

$$\epsilon = \int_0^L \frac{1}{n} \frac{dn}{dy} dz = \int_0^L \frac{\beta}{n\rho_s} \frac{d\rho}{dy} dz$$

Light Refraction Through a Gaseous Medium

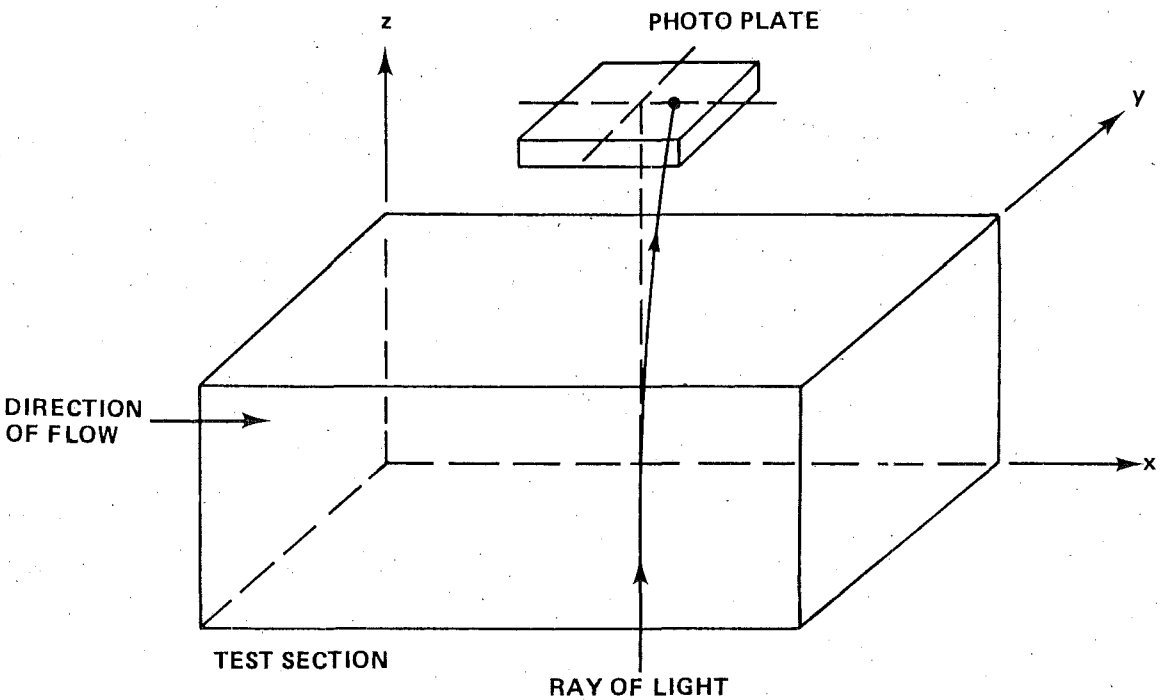

Flow is in the X direction. Light beam is in the Z direction.

$$\epsilon_y = \frac{1}{n} \int_0^L \frac{\partial n}{\partial y} dz = \frac{\beta}{n\rho_s} \int_0^L \frac{\partial \rho}{\partial y} dz$$

$$\epsilon_x = \frac{1}{n} \int_0^L \frac{\partial n}{\partial x} dz = \frac{\beta}{n\rho_s} \int_0^L \frac{\partial \rho}{\partial x} dz$$

The Schlieren

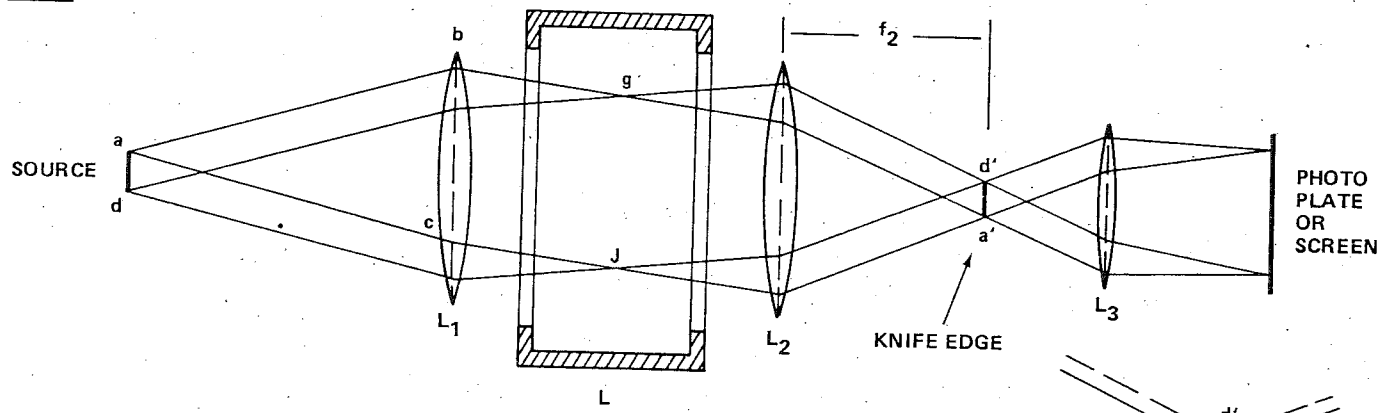

- A SCHLIEREN LENS SYSTEM PENCILS OF LIGHT SHOWN FOR UNIFORM DENSITY
- A KNIFE EDGE PLACED AT d'a' TO INTERCEPT THE LIGHT
- AT THE KNIFE EDGE THE Δy DISTANCE IS CAUSED BY REFRACTION $\Delta y = f_2 \epsilon$ (FOR SMALL ANGLES) f_z IS THE FOCAL LENGTH OF LENS L_2
- THE CONTRAST ON THE PHOTO PLATE $C = \frac{\Delta I}{I}$ ← ILLUMINATION

$$C = \frac{\Delta y}{y_1} = \frac{f_2 \epsilon}{y_1} \quad \text{WHERE } \epsilon = \frac{L}{n_1} \frac{dn}{dy}$$

$$C = \frac{f_2 L \beta}{n_1 y_1 \rho_s} \frac{d\rho}{dy}$$ ← TEST SECTION

$$\epsilon = \frac{L}{n_1} \frac{\beta}{\rho_s} \frac{de}{dy}$$

SINCE, $n = 1 + \frac{\beta \rho}{\rho_s}$

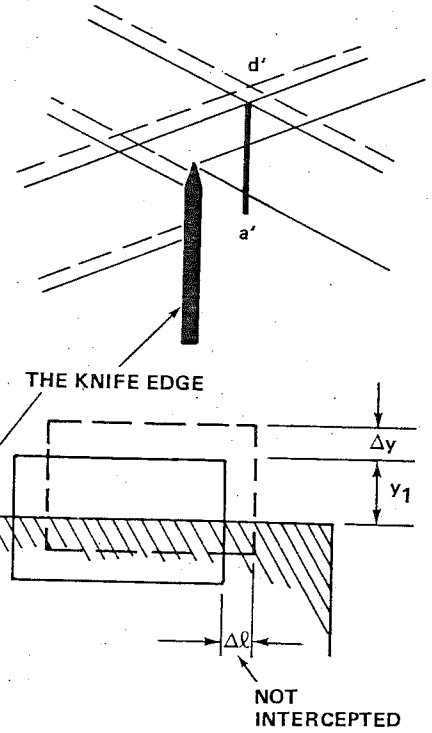

The Shadow Method

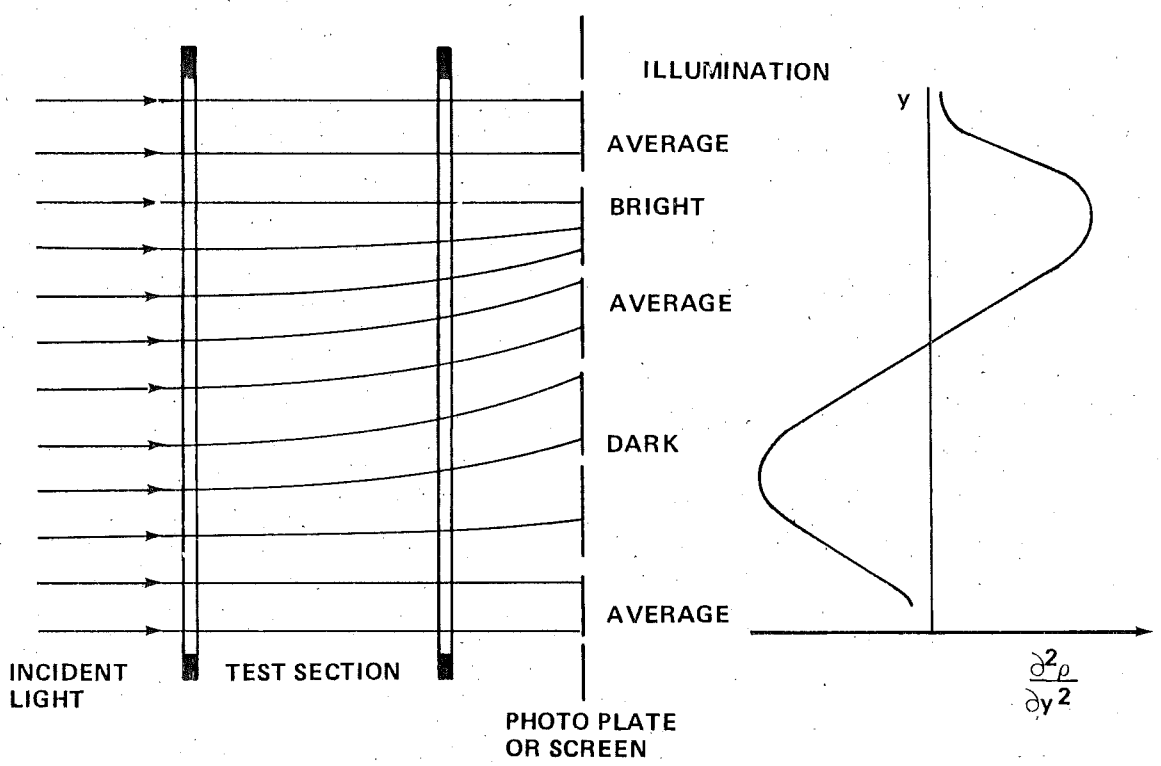

Shadow effect (dark and bright areas) depend on

$$\frac{\Delta \epsilon}{\Delta y} = \frac{\epsilon_2 - \epsilon_1}{y_2 - y_1}$$

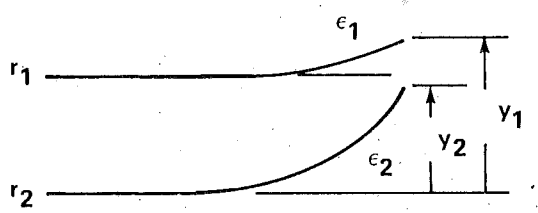

or on $\frac{\partial \epsilon}{\partial y}$

$$\epsilon = \frac{L\beta}{\rho_s} \frac{\partial \rho}{\partial y} \Bigg)$$ Test Section Section

$$\Delta I = \frac{\partial \epsilon}{\partial y}$$

$$= \frac{L\beta}{\rho_s} \frac{\partial^2 \rho}{\partial y^2}$$

or, in plane flow the illumination $\Delta I = \frac{\beta L}{\rho_s} \left[\frac{\partial^2 \rho}{\partial y^2} + \frac{\partial \rho^2}{\partial z^2} \right]$.

Appendix B.

INTERFEROMETRY AND HOLOGRAPHY FUNDAMENTALS

Interference Method - Fundamental Operations

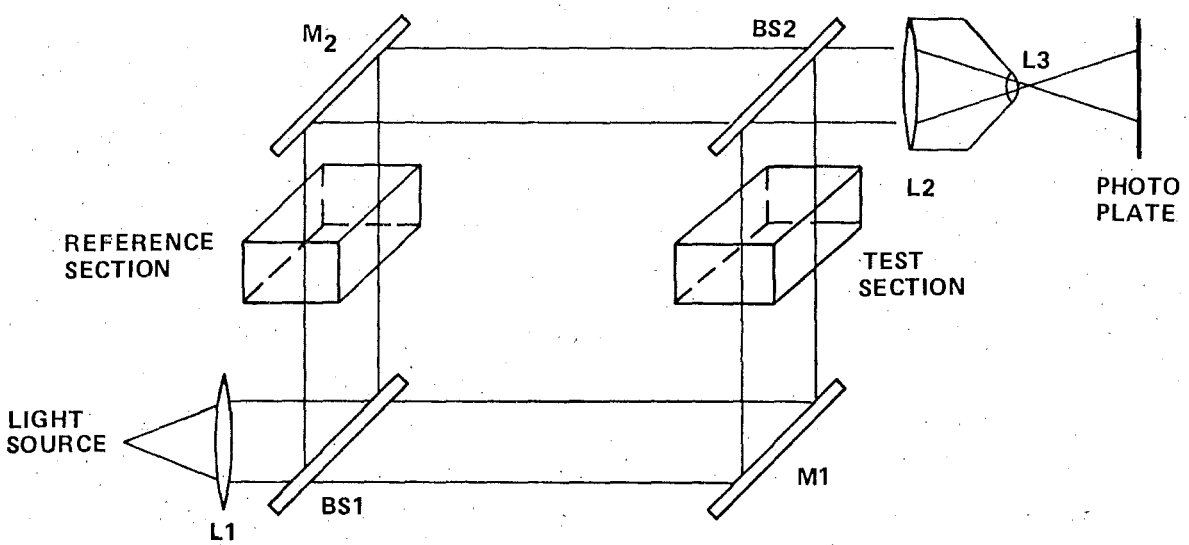

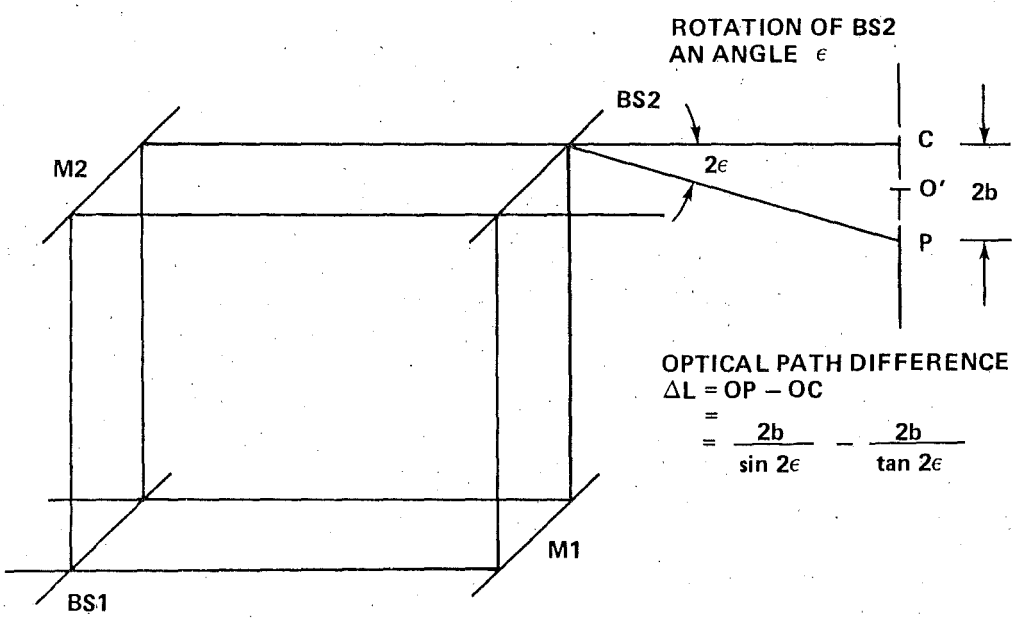

OPTICAL PATH DIFFERENCE

$\Delta L = OP - OC$

$= \frac{2b}{\sin 2\epsilon} - \frac{2b}{\tan 2\epsilon}$

$\Delta L = N\lambda = 2b\epsilon$

FRINGE WIDTH $= \frac{b}{N} = \frac{\lambda}{2\epsilon}$

Fringe and Density Relation

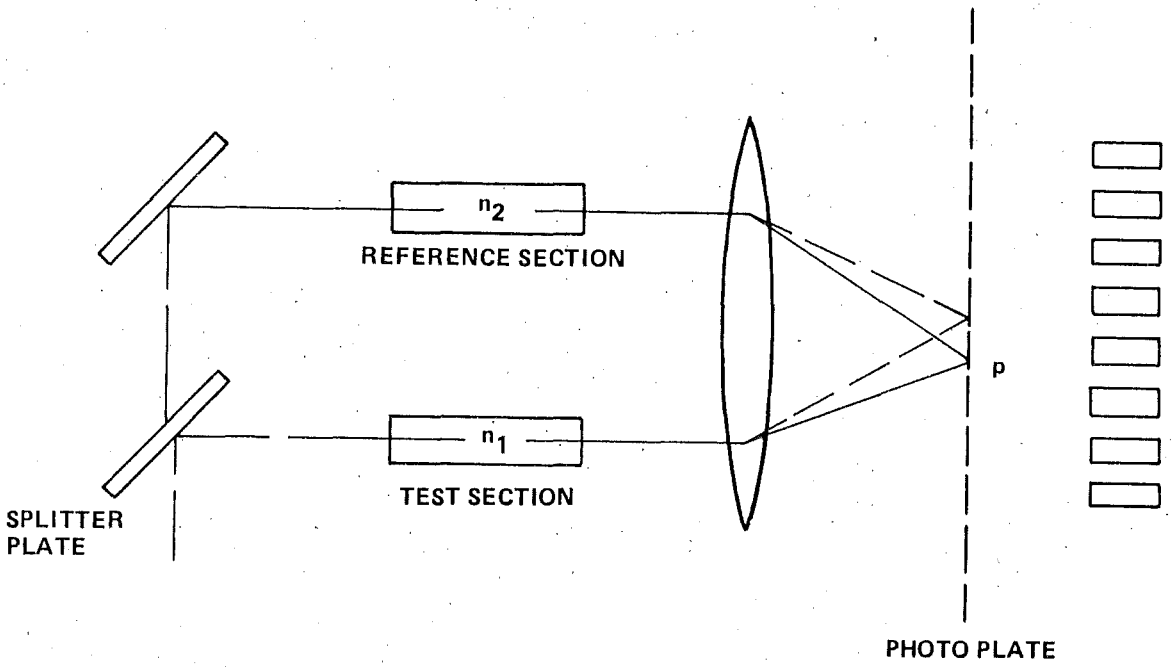

If $n_1 > n_2$, then $C_2 > C_1$

$$n_1 = \frac{C_0}{C_1} = 1 + \frac{\beta\rho_1}{\rho_s}$$

The additional time to traverse the test section is

$$n_2 = \frac{C_0}{C_2} = 1 + \frac{\beta\rho_2}{\rho_s}$$

$$\Delta t = \frac{L}{C_1} - \frac{L}{C_2} = \frac{L}{C_0}(n_1 - n_2).$$

Change in optical path is $\Delta L = C_0\Delta t = L(n_1 - n_2) = N\lambda$

$$N = \frac{L}{\lambda}(n_1 - n_2)$$

$$N = \frac{\beta L}{\lambda}\left(\frac{\rho_1 - \rho_2}{\rho_s}\right) = \text{number of fringes.}$$

If density varies along a ray

$$N = \frac{\beta}{\rho_s\lambda}\int_0^L (\rho_1 - \rho_2)ds \quad .$$

Sensitivity

Depends on brightness and uniformity of illumination and on an optical system that loses little light

Schlieren System

$$\text{Contrast } C = \frac{\Delta I}{I} = \frac{\Delta y}{y_1}$$

$$= \frac{f_2 \epsilon}{y_1} \quad .$$

$$\text{Sensitivity } s = \frac{C}{\epsilon} = \frac{f_2}{y_1} \quad .$$

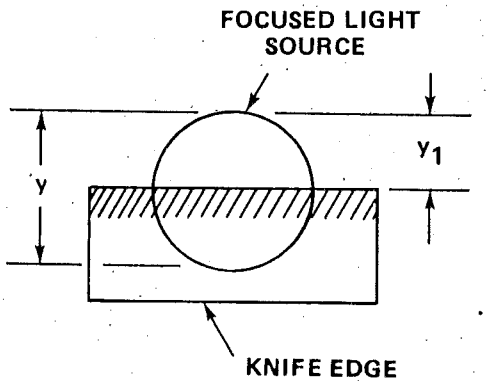

For AMC reproductive system using holograms

$y = 8 - 10$ microns

$f_2 \cong 25$ inches $\qquad s = 1.586 \times 10^5$

Interference and Holographic Methods

$$\text{Sensitivity } s = \frac{N}{\Delta\rho} = \frac{\beta L}{\lambda \rho_s}$$

$$= 1.563 \times 10^6 \ \frac{\text{fringes}}{\text{lbm/ft}^3}$$

For $\rho_s = 0.075$ lbm/ft^3 and

$\lambda = 0.4 \times 10^{-6}$ meters

$$s = 4.469 \times 10^3 \ \frac{\text{fringes}}{\text{lbm/ft}^3}$$

$\beta \cong 0.000293$

$L = 18$ inches $= 0.457$ meter

$\lambda = 0.4 \rightarrow 0.7 \times 10^{-6}$ meters

$\rho_s \cong 0.0002144$ lbm/ft^3

(for P = 20 torr, T = 1500°K)

Precision of the Interferometer

Approximate discernible fringe shift $\delta N = 0.1$ fringe. From a change in optical path

$$\frac{\beta L}{\rho_s} (\rho - \rho_s) = \lambda N \quad .$$

For delta changes

$$\frac{\beta L}{\rho_s} \delta\rho = \lambda \delta N$$

or

$$\delta\rho = \frac{\delta N}{s} \quad .$$

Density change for $\delta N = 0.1$ is

$$\delta\rho = \frac{0.1}{4.469 \times 10^3} = 2.23 \times 10^{-5} \text{ lbm/ft}^3 \quad .$$

Conditions:

$$\left\{ \begin{array}{l} \beta = 0.000293 \\ L = 0.457 \text{ meter} \\ \lambda = 0.4 \times 10^{-6} \text{ meters} \\ \rho_s = 0.075 \text{ lbm/ft}^3 \end{array} \right\} \quad .$$

NOMENCLATURE

A_e	Nozzle exit area
A_t	Nozzle throat area
A_t^*	Nozzle throat area for sonic flow at the throat
γ	Ratio of specific heats (C_p/C_v)
$\bar{M}$	Molecular weight
M_e	Nozzle exit Mach number
$\dot{m}_a$	Actual mass flow rate
$\dot{m}_c$	Calibrated mass flow rate
P_c	Cavity pressure
P_e	Nozzle exit pressure
P_j	Mass injection pressure
P_{m_c}	Center nozzle manifold pressure
P_{m_o}	Outside nozzle manifold pressure
P_o	Stagnation pressure
R	Gas constant
T_a	Actual temperature
T_c	Calibrated temperature
T_e	Nozzle exit temperature
T_{m_c}	Center nozzle manifold temperature
T_{m_o}	Outside nozzle manifold temperature
T_o	Stagnation temperature
V_e	Nozzle exit velocity
ρ_e	Nozzle exit gas density

BIBLIOGRAPHY

Chapman, A. J. and Walker, W. F., Introductory Gas Dynamics, HRW Series in Mechanical Engineering, Dallas, Texas, 1971.

Dohen, L. S. and Girole, R. N., Investigation of the Mixing and Combustion of Turbulent, Compressible Free Jets, George C. Marshall Space Flight Center, National Aeronautics and Space Administration, Marshall Space Flight Center, Alabama, December 1969, NASA CR-1473.

Hayday, A. A., Mixing Phenomena Related to CW Chemical Lasers, US Army Missile Command, Redstone Arsenal, Alabama, July 1971, Report No. RK-TR-71-16.

Hill, P. G. and Peterson, C. R., Mechanics and Thermodynamics of Propulsion, Adderson and Weley, Reading, Massachusetts, 1965.

Klimberg, J. M., Kubotn, Toshi, and Lees, Lester, "Theory of Exhaust - Plume/Boundary Layer Interactions of Supersonic Speeds," AIAA Paper No. 70-230, AIAA 8th Aerospace Sciences Meeting, January 1970.

Liepmann, H. W. and Roshko, A., Elements of Gasdynamics, John Wiley and Sons, Inc., New York, 1965.

Mirels, H., Hofland, R., and King, W. S., "Simplified Model of the CW Diffusion - Type Chemical Laser," AIAA 10th Aerospace Sciences Meeting, January 1972.

Schety, J. A., Unified Analysis of Turbulent Jet Mixing, George C. Marshall Space Flight Center, National Aeronautics and Space Administration, Marshall Space Flight Center, Alabama, July 1969, NASA CR-1382.

Zukoski, E. E. and Spaid, F. W., "Jet Penetration of Secondary Injections," AIAA Journal, 1969.

DISTRIBUTION

	No. of Copies
Defense Documentation Center Cameron Station Alexandria, Virginia 22314	12
University of California Los Alamos Scientific Laboratory Post Office Box 1663 ATTN: T. D. Butler, T3 Los Alamos, New Mexico 87544	1
Lockheed Missile and Space Company Huntsville Research and Engineering Center Post Office Box 1103 ATTN: Mr. John Benefield Huntsville, Alabama 35807	1
McDonnell-Douglas Research Laboratory P. O. Box 516 ATTN: Dr. Thomas J. Menne St. Louis, Missouri 63166	1
General Electric Post Office Box 8555 ATTN: Mr. M. J. Linevsky VFSC-L 9523 Philadelphia, Pennsylvania 19101	1
University of Mississippi Mechanical Engineering Dept. ATTN: Dr. C. R. Wimberly University, Mississippi 38677	5
General Motors Corporation Santa Barbara Operations 6767 Hollister Avenue ATTN: Dr. Martin Steinberg Goleta, California 93017	1
Bell Aerospace Company Post Office Box 1 ATTN: Dr. W. C. Solomon Buffalo, New York 14240	1
TRW Systems Group 1 Space Park ATTN: Dr. T. Jacobs Redondo Beach, California 90278	1
Mitre Corporation Post Office Box 208 ATTN: Dr. A. Cron Mail Stop A-130 Bedford, Massachusetts 01730	1
Massachusetts Institute of Technology Lincoln Laboratory 244 Wood Street ATTN: S. Edelberg Lexington, Massachusetts 02173	1
Naval Research Laboratory ATTN: Dr. Bill Watt Dr. R. Kagarise Washington, D.C. 20390	1 1
Director Advanced Research Projects Agency ATTN: Dr. Ed Gerry Technical Information Office Washington, D.C. 20301	1 1
Commander US Army Materiel Command ATTN: AMCRD-PT AMCRD-TP 5001 Eisenhower Avenue Alexandria, Virginia 22304	1 1
Battelle Memorial Institute 505 King Avenue ATTN: Battelle-STD-IC Columbus, Ohio 43201	1
Raytheon Company Research Division ATTN: Dr. Frank Horrigan Waltham, Massachusetts 02154	1
Naval Ordnance Laboratory White Oak ATTN: Dr. Leon H. Schindel (Code 310) Silver Spring, Maryland 20910	1
Riverside Research Institute 632 West 125th Street ATTN: Dr. L. H. O'Neill New York, New York 10027	1
North American Rockwell Corporation 6633 Canoga Avenue ATTN: S. V. Gunn Canoga Park, California 91304	1
Commander Harry Diamond Laboratories ATTN: AMXDO-RCB, Dr. J. Wemarich Washington, D.C. 20438	1
Commander US Army Research Office-Durham Box CM, Duke Station ATTN: Dr. Robert J. Lontz Durham, North Carolina 27706	1
Chief of Research and Development Department of the Army Army Research Office ATTN: Dr. Robert B. Watson Washington, D.C. 20310	1
Commander Rock Island Arsenal Research Laboratory US Army Weapons Command ATTN: SWERI-RET-E, Dr. W. McGarvey Rock Island Arsenal, Illinois 61201	1
Commander Frankford Arsenal ATTN: SMUFA-N-5300, Dr. Wm. McNeil SMUFA-W-1000, Joint Laser Safety Team Philadelphia, Pennsylvania 19137	1 1
Commander US Army Picatirny Arsenal Bldg 1515 ATTN: SMUPA-VL, Mr. P. Kisatsky Dover, New Jersey 07801	1
Commander US Army Materiels and Mechanics Research Center ATTN: AMXMR-P, Mr. Katz Watertown, Massachusetts 02172	1
Commander US Army Combat Development Command Chemical Bilogical and Radiological Agency ATTN: CSGCB-ST, Mr. H. P. Whitten Fort McClellan, Alabama 36201	1
Advisory Group on Electron Devices 201 Varick Street ATTN: Secretary, SP GP on Optical Masers New York, New York 10014	1

	No. of Copies
Commander US Army Ballistic Research Laboratories ATTN: AMXRD-BSP, Dr. E. Alcaraz AMXRD-BTL, Mr. F. J. Allen Aberdeen Proving Ground, Maryland 21005	1 1
Martin-Marietta, Denver Division Post Office Box 179 ATTN: Mr. S. Chapin Denver, Colorado 80201	1
School of Mechanical Engineering Purdue University ATTN: Dr. James G. Skifstad Lafayette, Indiana 47907	1
Avco Everett Research Laboratories 2385 Revere Beach Parkway ATTN: Dr. Jack Wilson Everett, Massachusetts 02149	1
Aerospace Corporation P. O. Box 95085 Attn: W. Warren El Segundo, California 90045	1
United Aircraft Research Laboratories 400 Main Street ATTN: Dr. George McLafferty East Hartford, Connecticut 06108	1
Hughes Research Laboratories 3011 Malibu Canyon Road ATTN: Dr. Peter Clark Malibu, California 90265	1
Air Force Weapons Laboratory ATTN: AFWL-LRT -SYT Kirtland Air Force Base New Mexico 87117	2 2
Commander US Army Electronics Command ATTN: AMSEL-KL-DT, Mr. B. Louis AMSEL-XL-S, Dr. R. Buser Fort Monmouth, New Jersey 07703	1 1
Cornell University 237 Phillips Hall ATTN: Dr. Cool Dr. Wolga Ithaca, New York 14850	1 1
Accurex Corporation Aerotherm Division 458 Clyde Avenue ATTN: Dr. Robert Kendall Mountain View, California 94040	1
Aerojet General Corporation Liquid Rocket Operations P. O. Box 15847 ATTN: Mr. F. Childs Sacramento, California 95813	1
Rand Coporation 1700 Main Street ATTN: Dr. H. Watonabi Santa Monica, California 90401	1
Pratt and Whitney Aircraft Florida Research and Development Center P. O. Box 2091 ATTN: Mr. T. Paras West Palm Beach, Florida 33402	1

	No. of Copies
The Boeing Company Scientific Research Laboratories 775 East Marginal Way ATTN: Dr. McClure Seattle, Washington 98124	1
Calspan Corporation 4455 Genessee Street ATTN: Dr. Charles Treanor Buffalo, New York 14221	1
Air Force Office of Scientific Research 1400 Wilson Boulevard ATTN: SRC, Dr. D. Ball Arlington, Virginia 22209	1
Hughes Aircraft Company Centinela and Teale Streets ATTN: Mr. E. R. Peressini Building 6, Mail Station E 125 Culver City, California 90230	1
AMSMI-IPWC -FR, Mr. Rives -O -R, Dr. McDaniel Mr. Fagan -RK, Dr. Rhoades Mr. Thorn -RKL, Dr. Wharton -RR, Dr. Hallowes -RRP, Dr. Barr -RX, COL Morrison -RB, Dr. Kobler -RBL -RPR -RK (Record Set)	1 1 1 1 1 1 5 1 1 1 1 1 5 1 1